UNIVERSIDAD DE CHILE

FACULTAD DE CIENCIAS FÍSICAS Y MATEMÁTICAS

DEPARTAMENTO DE GEOLOGÍA

EVOLUCIÓN DE LA DINÁMICA SEDIMENTARIA Y SUS IMPLICANCIAS PALEOCLIMÁTICAS DURANTE EL HOLOCENO TEMPRANO DEL VALLE DEL RÍO TURBIO, ANDES SEMIÁRIDOS DE CHILE (30°S)

TESIS PARA OPTAR AL GRADO DE MAGÍSTER EN CIENCIAS MENCIÓN GEOLOGÍA

MARION ARLETTE SAN JUAN DÍAZ

Profesora guía:
Valentina Flores Aqueveque

Profesora co-guía:
Tania Villaseñor Jorquera

Miembros de la comisión:
Antonio Maldonado Castro
Luisa Pinto Lincoñir

Esta tesis ha sido financiada por el Proyecto Fondecyt Regular N°118041

Santiago de Chile
2023

RESUMEN
TESIS PARA OPTAR AL: Grado De Magister En Ciencias, Mención Geología
POR: Marion Arlette San Juan Diaz
FECHA: 2023
PROFESORA GUÍA: Valentina Flores Aqueveque

EVOLUCIÓN DE LA DINÁMICA SEDIMENTARIA Y SUS IMPLICANCIAS PALEOCLIMÁTICAS DURANTE EL HOLOCENO TEMPRANO DEL VALLE DEL RÍO TURBIO, ANDES SEMIÁRIDOS DE CHILE (30°S)

El valle del río Turbio se ubica en la zona cordillerana de la región de Coquimbo en Chile central, y se enmarca en un actual clima semiárido condicionado por la dinámica de la circulación atmosférica del Sudamérica. Diversos estudios interpretan variaciones en las condiciones climáticas desde el último máximo glaciar hasta el Holoceno, pero son limitados los estudios que reconstruyen la evolución de los ambientes sedimentarios como consecuencia de las variaciones climáticas. El presente estudio pretende reconstruir las condiciones paleoambientales y sus implicancias climáticas, mediante el estudio de la evolución de la dinámica sedimentaria desde un régimen paraglaciar a fluvial durante el Holoceno, en los Andes semiáridos del norte de Chile central, el Valle del Río Turbio. Se realizó un estudio sedimentológico, geoquímico y cronoestratigráfico de detalle de las sucesiones sedimentarias ubicadas en las quebradas Los Piuquenes, y El Calvario. De esta manera, se identificaron ambientes sedimentarios de tipo aluvial, fluvial y lacustre, en donde la dinámica de los procesos sedimentarios estaría condicionada por el régimen hidrológico, y éste a su vez ha sido controlado por el clima en el pasado. El conjunto de la información nos permitió interpretar y comparar las condiciones climáticas entre los 11000–2200 años cal BP, los cuales fueron correlacionados con los antecedentes paleoclimaticos regionales durante el Holoceno.

AGRADECIMIENTOS

A mi madre, padre, hermana y hermano, incondicionales hasta el final. Si se que alguien siempre estará ahí, son ellos…Gracias inmensas por criarme con ese amor y rigurosidad que les caracteriza. A mis primas queridas, tremendas mujeres, compañeras y amigas, que aún me siguen esperando para poder vernos, porque a veces la vida académica/profesional nos amarra y no nos deja salir mucho… Ya estoy terminando y ya vamos a brindar jaja

Pero no todo es familia, debo y quiero hacer mención a mis grandes mentoras, Tania, Valentina, Pia, Luisa, no sé ni como ordenarlas porque cada una toma un rol significativo en mi vida profesional y académica. Gracias por sus enseñanzas, su paciencia, por considerarme, por corregirme jeje ¡Siempre les estaré agradecida y me jactare de tener a las mejores profes de la vida!

Gracias a mis amigos y amigas, que siempre supieron alegrar esos momentos de estrés con sonrisas y buenas platicas, les llevo en mi corazón.

También mencionar aquellas personas que apañaron en los terrenos ¡cómo no contarlos! Gracias por sus ideas, su buena voluntad, por sus discusiones y enseñanzas. Agradezco el apoyo de Antonio y a les chiques del Ceaza, sin ustedes nada de esto estaría pasando.

Muy agradecida estoy, de todos, de todo, incluso de mi…

TABLA DE CONTENIDO

INDICE DE FIGURAS

1. INTRODUCCIÓN

La región semiárida en Chile central (~ 30°S–34°S) se encuentra en la una zona de transición climática, denominada como la Diagonal Árida Sudamericana (DA) y se enmarca entre dos regiones con climas contrastantes, por el norte un clima árido e hiperáridos, y por el sur un clima mediterráneo (37°S) a húmedo (~42°S), donde las precipitaciones aumentan hacia las latitudes más altas (45°S) (Miller, 1976). En las regiones con climas áridos e hiperáridos (~17°S–30°S) la intensificación de las precipitaciones tiene lugar en los meses de verano austral (Diciembre–Enero–Febrero) debido al Sistema Monzónico Sudamericano (SAMS–South American Monsoon System) (e.g., Garreaud et al., 2003). Mientras que en las regiones semiáridas (~30°S – 34°S) ocurren durante el invierno austral (Junio–Julio–Agosto) como consecuencia del debilitamiento y migración hacia el ecuador del Anticiclón Subtropical del Pacífico Suroriental (ASPS) (Figure 1.1). Este debilitamiento permite que los frentes de tormenta atraídos por el cinturón de vientos del suroeste (SWW-Southern Westerly Wind), alcancen latitudes más bajas (e.g. Garreaud et al., 2009; Quintana y Aceituno, 2012). Esta variabilidad interanual de las precipitaciones invernales también se ven influenciadas por los fenómenos oceánico-atmosféricos naturales que se sobreponen a las condiciones normales, como son El Niño Oscilación del Sur (ENOS) y la Oscilación Decadal del Pacífico (ODP), provocando cambios en las condiciones climáticas cada cierto número de años.

Debido a que el margen continental entre las costas de Chile-Perú se ubican en una zona de transicional entre condiciones atmosféricas intertropicales hacia el ecuador y extratropical hacia el polo, junto con la fuerte influencia de las corrientes océanicas en el clima, estas regiones son un lugar ideal para el estudio de las variaciones atmosféricas pasadas en el extremo sur de América. Por lo que diversos estudios se han desarrollado en el área, entregando como resultado el comportamiento y evolución de los componentes de la circulación oceánica-atmosférica y de esta manera, las variaciones climáticas desde el último máximo glaciar hasta el Holoceno, relacionando e identificando periodos climáticos secos y húmedos (*e.g*. Vargas et al., 2006; Ortega et al., 2012, 2019; Jenny et al., 2002; Maldonado y Villagrán, 2006; Villa-Martinez et al., 2003; Cabré et al., 2017; Tiner et al., 2018) además de intentar dilucidar los efectos de los fenómenos interanuales como el ENOS y la ODP.

Diversos *proxies* paleoclimáticos se han utilizado en las reconstrucciones paleoclimáticas, entre ellos se encuentra el estudio de los sedimentos como indicadores de intensidad de procesos físicos del ambiente. Tal como son los procesos sedimentarios, estos se encuentran intrínsicamente relacionados con las condiciones climáticas preexistentes en el ambiente, por ejemplo, el aumento de las precipitaciones y temperaturas puede desencadenar eventos de flujos superficiales de alta energía, que si prevalecen pueden modificar el régimen hidrológico. Por lo tanto, los sedimentos

transportados y depositados en el sistema son un registro directo de la energía, intensidad e interacción de los procesos sedimentarios. De esta manera, la acumulación de los sedimentos representa la sedimentación durante un periodo de tiempo, y a su vez queda el registro de la dinámica asociada al ambiente sedimentario.

Pese a que se han realizado diferentes trabajos que contribuyen en la reconstrucción paleoclimatica en las regiones semiáridas, poco se ha hablado de como los ambientes sedimentarios se han visto afectados y modificado por los cambios del clima, de esta manera es que se proponer reconstruir la dinámica sedimentaria paleoambiental en uno de los principales ríos de la cuenca alta del Río Elqui, el valle del Río Turbio. Para ello se estudiaron los depósitos sedimentarios aterrazados del Río Turbio, ubicado en la parte alta de los Andes semiáridos del centro-norte de Chile (~30°S). El registro sedimentario data desde Pleistoceno Tardío-Holoceno temprano al Holoceno tardío (Riquelme et al., 2011; Houbart, 2014), siendo un muy buen indicador de las condiciones ambientales-climáticas que prevalecieron durante dicho periodo de tiempo. Ha sido posible comparar los resultados obtenidos en este trabajo con los escenarios climáticos interpretados para la región (e.g., Riquelme et al, 2011; Tiner et al., 2018). Dichos estudios, junto con la cronología de los eventos depositacionales, nos permiten reconstruir la evolución paleoambiental del valle del Río Turbio y las posibles implicancias climáticas durante el Holoceno.

1.1 Hipótesis

Las sucesiones sedimentarias holocenas del valle del Río Turbio (~30°S) representa la evolución de la dinámica sedimentaria del sistema fluvial durante el Holoceno, las cuales a su vez fueron condicionadas por la variabilidad del clima en los Andes Semiáridos durante dicho periodo tiempo.

1.2 Objetivos

1.2.1 Objetivo General

Analizar las asociaciones de facies y la proveniencia de los depósitos fluvio-aluvial del Holoceno en el valle del Río Turbio, para reconstruir la evolución de los procesos sedimentarios e interacción con el ambiente y clima que prevalecieron durante dicho periodo en los Andes Semiáridos Chile.

1.2.2 Objetivos específicos

(1) Definir asociaciones de facies para interpretar los procesos sedimentarios y la interacción con el paleo-ambiente sedimentario.
(2) Caracterizar la geoquímica de los sedimentos que permitan identificar posibles áreas fuente de los sedimentos.
(3) Determinar la edad de los sedimentos para reconstruir la evolución de los procesos sedimentarios en el/los paleoambientes.

(4) Atribuir los cambios en la dinámica de los procesos sedimentaria a posibles escenarios climáticos y así correlacionar con las características climáticas del Holoceno

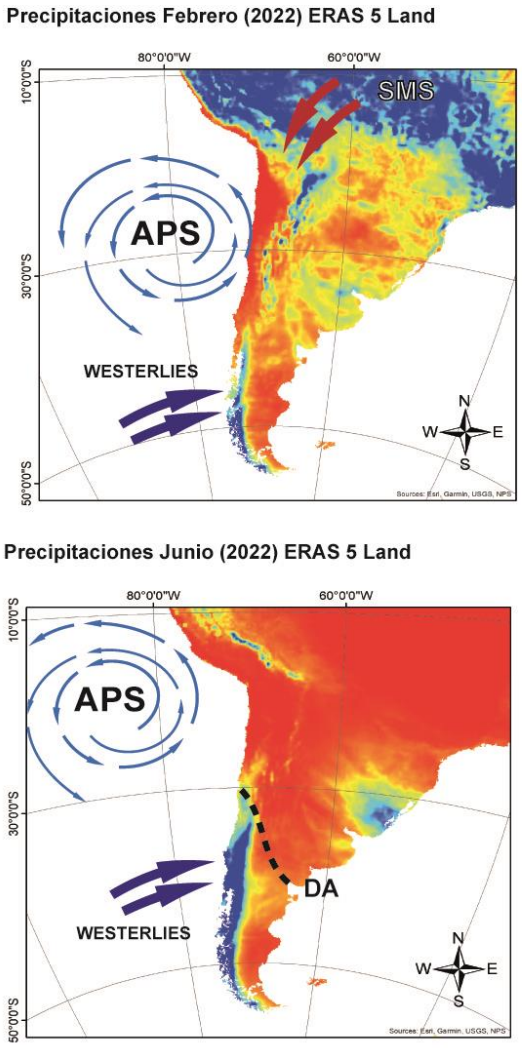

Figure 1.1. Características principales de la circulación atmosférica estacional el hemisferio sur (SMS: Sistema Monzónico Sudamericano y Westerlies: Cinturón de Vientos del Suroeste). La línea de punteada indica la posición de la Diagonal árida sudamericana.

1.3 Ubicación y accesos

El área de estudio comprende el segmento El Calvario – Los Piuquenes en el valle del Río Turbio (29°57'15.41"S - 70°10'34.28"O), uno de los principales afluentes del Río Elqui. Este valle se ubica en la Cordillera Principal de los Andes chilenos, en la Comuna de Vicuña, Provincia de Elqui, Región de Coquimbo al norte de Chile central (Figura 1.1). Desde Santiago de Chile, se accede por la Ruta 5 en dirección norte hasta llegar a la ciudad de La Serena, para luego continuar 131 km por la Ruta 41 hacia Vicuña. La zona de estudio se encuentra 70 km al oeste del paso fronterizo Aguas Negras en el sector Miraflores.

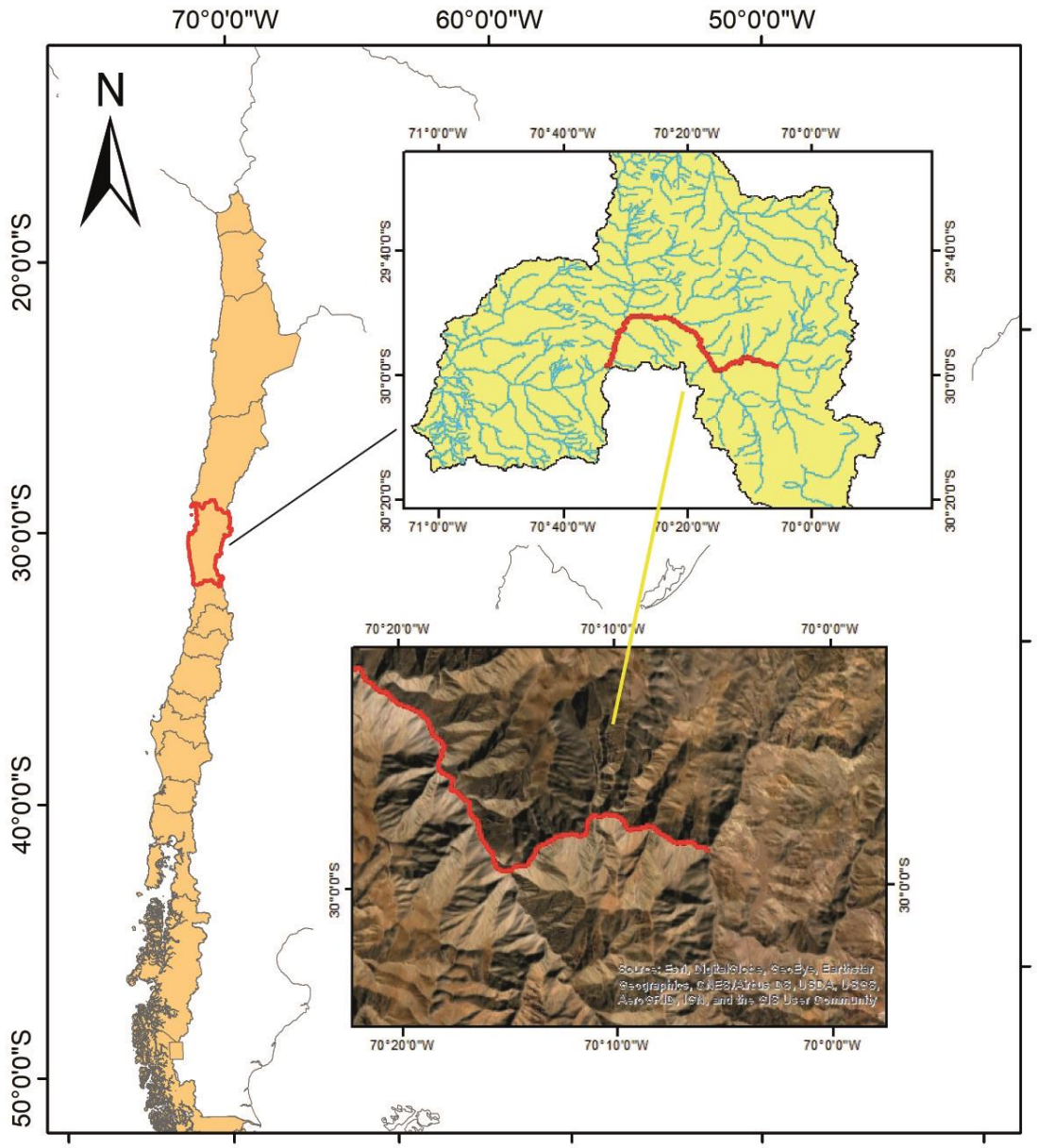

Figura 1.1. Mapas de ubicación región de Coquimbo y comuna de Vicuña. A) Mapa con redes de drenaje (líneas celestes) de la comuna de Vicuña, línea roja representa la ruta F-41; B) Ubicación de afloramientos principal de zona de estudio (cuadro rojo).

2 METODOLOGÍA

2.1 Trabajo en Terreno

Se realizaron salidas 3 a terreno en los años 2020 y 2022, a la zona de estudio, donde se reconocieron y describieron detalladamente las características de los sedimentos, se visualizaron las relaciones de contacto y la disposición espacial entre las unidades estratigráficas. Todo esto mediante la elaboración de columnas y perfiles estratigráficos a escala 1:100 en un total de 4 afloramientos, un afloramiento principal y tres secundarios.

Se recolectaron muestras de las diferentes capas de sedimentos, para el análisis sedimentológico y composicional, y un total de 6 muestras de capas ricas en materia orgánica para dataciones por radiocarbono.

2.2 Trabajo de Laboratorio

Dataciones por radiocarbono

Para determinar la cronología de los eventos se tomaron muestras en los distintos niveles de sedimentos ricos en material orgánico que fueron datados mediante el método de radiocarbono (C14), en el laboratorio DirectAMS con el método AMS. Al obtener la edad estas fueron calibradas en el programa Calib Rev 8.1.0 utilizando la curva de calibración SHCal 20, para el hemisferio sur. Con ello se puede delimitar el intervalo de edades de los sedimentos que se encuentran entre las capas carbonosas.

Análisis granulométrico

El porcentaje de tamaños de partículas inferiores a 1 mm se obtuvo mediante el analizador de partículas por difracción láser Mastersizer 2000 de Malvern, equipado con una unidad de dispersión Hydro MV (Malvern Instruments Limited, Malvern, Reino Unido). Previo al análisis de difracción láser, los sedimentos fueron tamizados, utilizando los tamices No. 10 y No. 18, para evitar que entren partículas mayores a 2 mm al equipo. Se ocuparon alrededor de 3-4 gr de sedimentos por muestra pasando tres veces a través del sistema de celdas Malvern, entregando un promedio de los tres análisis.

Posteriormente, se obtuvieron los gráficos de distribución y frecuencia acumulada y se calcularon los parámetros estadísticos sedimentológicos: media (M), desviación estándar (selección) (SD), curtosis (K), simetría (SK) y percentiles (D10, D50 y D90) utilizando el programa Gradistat (Blott, 2001) que calcula los parámetros estadísticos mediante el método de momentos de Folk y Ward (1964).

2.3 Trabajo de Gabinete

En primer lugar, se digitalizaron las columnas y esquemas estratigráficos, atendiendo a las descripciones en terreno y la fotointerpretación de los afloramientos. Posteriormente, se identificaron las facies sedimentarias, según la clasificación granulométrica y las características de ordenamiento interno de los sedimentos, luego se interpretaron las asociaciones de facies e identificaron los elementos arquitecturales en los perfiles estratigráficos. De esta forma, y junto a los datos cronológicos, se pretende interpretar la evolución de los eventos depositacionales en los cambios verticales y laterales de facies de las sucesiones estratigráficas.

3 RESULTADOS

A continuación, los resultados del trabajo de tesis se presentan siguiendo el formato de un artículo científico, el cual será sometido en una revista científica junto con los nuevos resultados que se han obtenido del proyecto Fondecyt regular n°1180413, titulado 'Climate change and landslides occurrence in the subtropical Andes since the Late Pleistocene'.

EVOLUTION OF SEDIMENTARY PROCESSES AND ITS PALEOCLIMATIC IMPLICATIONS DURING THE HOLOCENE OF THE TURBIO RIVER VALLEY, SEMI-ARID ANDES, CHILE (30°S)

M. San Juan[1]; V. Flores[1]; Tania Villaseñor[2]; A. Maldonado[3]

[1]Departamento de Geología, Universidad de Chile, Plaza Ercilla 803, Santiago, Chile

[2]Instituto de Ciencias de la Ingeniería, Universidad de O'Higgins, Libertador Bernardo O'Higgins 611, Rancagua, Chile

[3]Centro de Estudios Avanzados en Zonas Áridas, Ossandón 877, Coquimbo, Chile

ABSTRACT

The sedimentary deposits of the Turbio River valley, located in Andean semiarid region in north-central Chile, reveal the fluvial dynamics of the river history during the Late Pleistocene to Holocene. In this research was recognizing the ancient paleoenvironment evolution and the dynamics of their sedimentary processes to interpret the influence of Holocene climate changes. For that we investigate the sedimentary mechanism producing those sedimentary environmental change to evaluate the paleoclimate significance.

A detailed sedimentological, geochemical, and chronostratigraphic study of the sedimentary successions located in the Los Piuquenes and El Calvario streams was carried out. Our results indicate the development of sheet flood, over bank flooding, detachment lake and debris flow, associated with an alluvial plain, channel river and alluvial fan paleoenvironments interaction. Thar processes would be conditioned by the hydrological regime, which in turn has been controlled by the climate in the past. The information allowed us to interpret and compare climatic conditions between 11000-2200 cal yr BP, which were correlated with regional paleoclimatic antecedents during the Holocene. A humid period was identified at the beginning of the Holocene, which lasts until 7500 yr cal BP, followed by dry conditions between 7500-5,500 yr cal BP. Then an increase in storm events between 5,500-4,100 yr cal BP was observed, followed by a relatively drier period between 4,100 - 2200 yr cal BP, and then a wetter period until the present day after 2200 yr cal BP.

1 INTRODUCTION

The Chilean continental margin provides a key region to study the natural variability of the climate and the change of the atmospheric and oceanic circulation teleconnection of the Southern Hemisphere, which include the Intertropical Convergence Zone (ITCZ), the Southern Westerly Wind belt (SWW) and the Antarctic Circumpolar Current (ACC) (Figure 1.1). The study area is in the Andean semiarid region north-central Chile (Figure 1.2), located in a transitional climate zone called South American Arid Diagonal (AAD) and between the arid to hyperarid Atacama Desert and Mediterranean central Chile. To the north of ADD (Atacama Desert) the precipitation occurs during the austral summer and is associated with the tropical monsoon season, whereas to the south (Mediterranean central Chile) rainfall concentrates mainly in the winter, controlled by the westerlies regime related to the strength and position of the South Pacific Subtropical High (SPSH) (Garreaud et al., 2008) (Figure 1.1). Interannual rainfall variability is strongly linked to the El Niño-Southern Oscillation (ENSO) and Pacific Decadal Oscillation (PDO) an atmospheric and oceanic phenomenon that produce change in the strength and position of the Subropical High Pressure cell (STH) (Montecinos and Aceituno 2003; Ruttlant and Fuenzalida 1991).

In the Andean Mountain range, major river systems are highly sensitive to climatic change and tectonism, both capable to modify the hydrodynamic conditions, therefore variations in the hydrologic regime along tropical and subtropical continental margins depend strongly on changes in regional ocean-atmosphere climate conditions. Several research explain the impact of latest Pleistocene-Holocene climate changes on hydrologic regime variations along the subtropical western margin of South America (e.g. Grosjean et al., 1997, 2001; Jenny et al., 2002; Vargas et al., 2006; Pueyo et al., 2011; Maldonado and Villagran, 2006; Moreno et al., 2010). Their observation has explained change in climate proxies from latitudinal shift and/or intensity variations of major atmospheric circulation features affecting western South America. This highlights the motivation of understanding how the sedimentary dynamics, due the hydrological regimen changes in the fluvial catchment, respond to regional and global climate drivers during the Holocene.

The sedimentological analysis is a useful tool for understand the hydrological change in the fluvial history, so the sedimentary successions an invaluable record of the environmental changes in the past. Sediments produced in a fluvial catchment reflect the velocity flow, turbulence, and regimen flow, as well as the mineralogical and geochemical of clastic sediment the lithology of the source (Grantham and Velbel, 1988; Garzanti et al., 2010, 2011; Dixon et al., 2012). Grain size analysis, also provide valuable data to understanding and defining the hydrodynamic mechanisms, and sediment provenance (Sahu et al., 1964; Blott., et al., 2001; Boggs 2009; Baiyegunhi et al. 2017). In the Andean semiarid region, the Turbio River valley contain fluvial sedimentary succession, that represent the river history from the last maximum-glacier to the Holocene (Figure 1.2) (e.g., Maldonado et al., 2006; Riquelme et al., 2011, Houbart, 2014; Honores, 2021, and

Calderon, 2021). This sedimentary record comprises by alluvial, glacial, lacustrine, and fluvial sedimentary succession as a fluvial terrace.

In this work is proposed a detailed stratigraphic, sedimentological, geochemical, and chronostratigraphic studies in the sedimentary deposits at the Tubio Valley. Through facies analysis, and recognizing of architectural elements and boundaries surface, can be interpreted the paleo sedimentary processes. As proposed Miall´s research (e.g, 1978, 1996, 2014, 2022) that permit us to interpret the sedimentary processes, and other hydrodynamic features in an ancient environmental system. The chronostratigraphic data helps us to correlate these extreme wets events, with other identified in the region. Finally, we aim to reconstruct the paleoenvironment evolution as the result of climate change during the Holocene in a semiarid climate mountainous scenario.

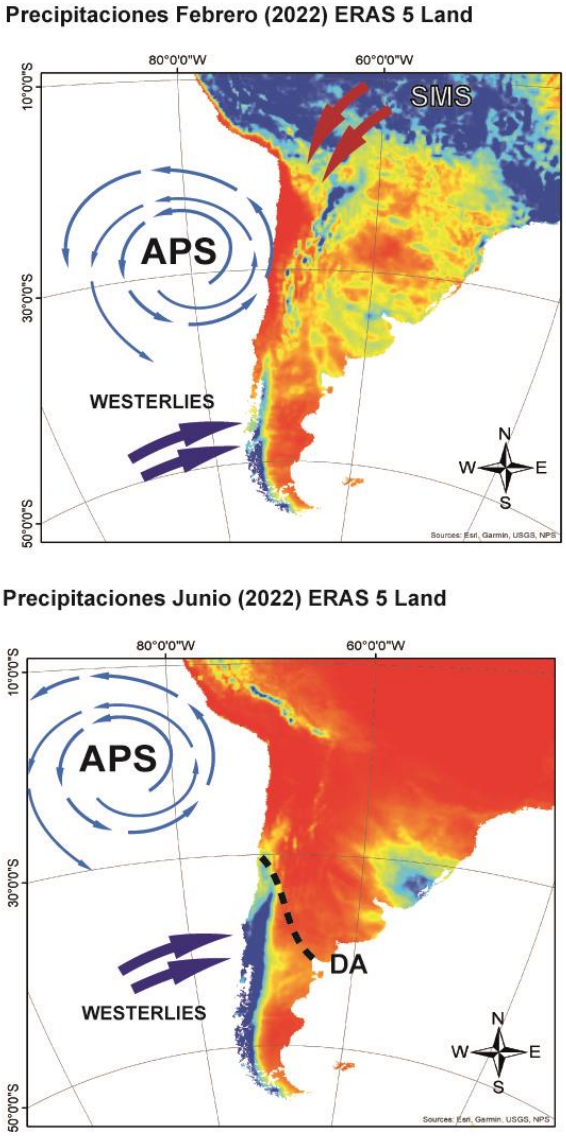

Figure 1.1. Precipitation maps during February and July, representing the austral summer and winter, respectively. The figure also presents the principal component of the atmospheric circulation in the south America.

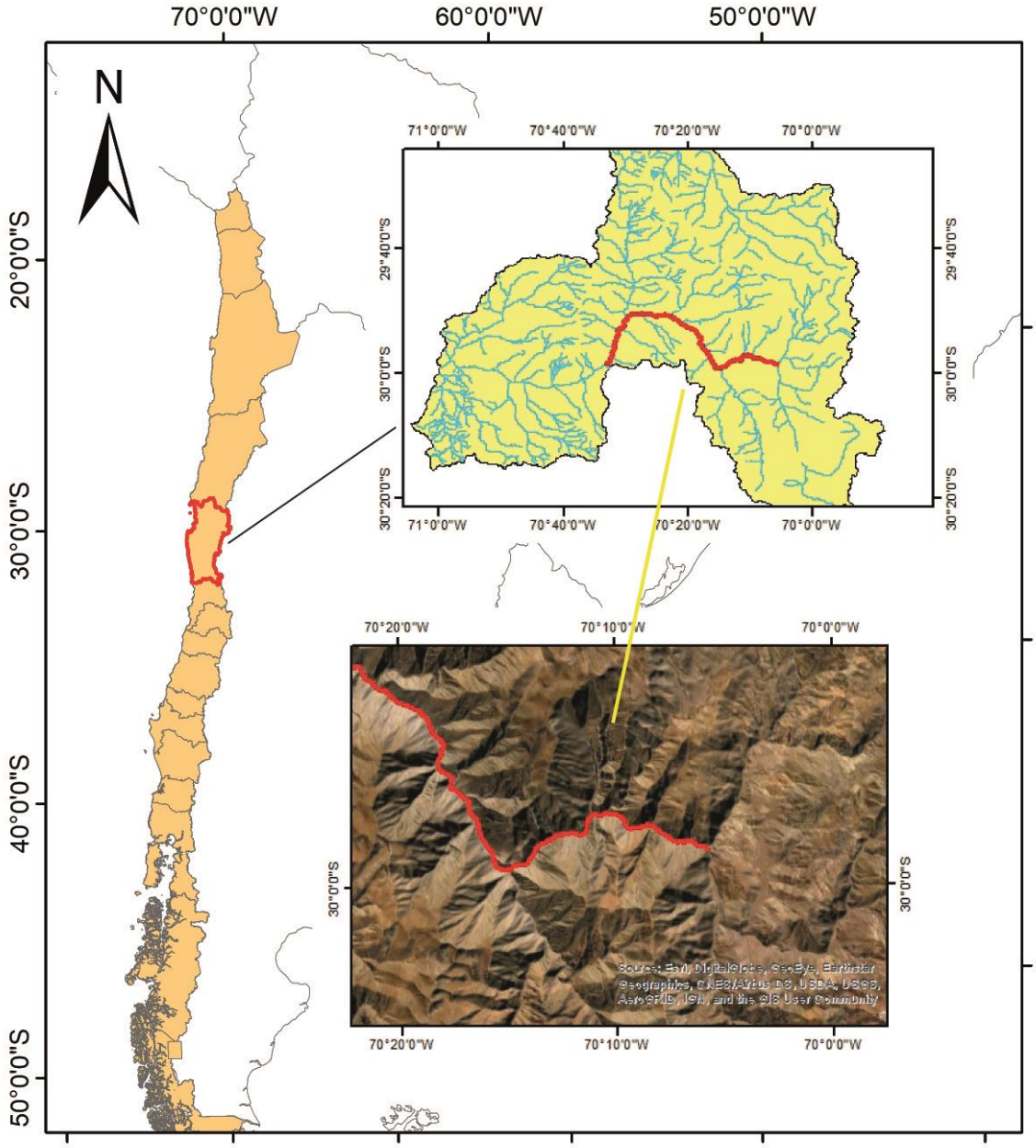

Figure 1.2. Location of Turbio valley, in the Coquimbo region, Chile. A-B trace show the principal creek and name of the outcrop studies

1.1 Geological and geomorphological setting

In the Chilean Frontal Cordillera ~ 30°S, large volumes of igneous and volcano-sedimentary Late Paleozoic to Mesozoic age are exposed as N-S parallel rock belts (Sernageomin., 2005). A simplified geological map of the Elqui catchment basin, in Vicuña province is in Figure 1.3. The oldest igneous rocks are concentrated in the western belt and the youngest in the eastern belt. Intermediate granitic, calc-alkaline rocks as granites, granodiorites, tonalites and diorites comprises the plutonic units (Elqui-Limarí batholith: Nasi et al., 1985; Marin et al., 1995). Those igneous rocks surface is in the middle of the

main catchment basin, while the upper basin is over a north-south trending volcanic and volcano-sedimentary rock, mainly andesitic, basaltic and pyroclastic types (Pastos blancos group). Limestones and marine siliciclastic rocks are presents, but with very limited surface exposure.

The Elqui basin located in the so-called Transversal Valleys segment (28-33°S) constitute one of the main basins in Coquimbo region. The Elqui river flows westward from the Andes Mountains to the Pacific Ocean and their principal tributaries rivers is Turbio and Claro rivers. The Turbio River is fed by Toro and La Laguna rivers (Figure 1.3). The availability of the stream-surface water depends mainly to the melting snow, rain precipitation, and less glacial fusion, that is more important in the La Laguna River.

Toro River located to the northeast Elqui basin through igneous, intrusive, and continental clastic rocks surface (Figure 1.3). Those petrological units host a large number of hydrothermal ore deposits, although only Cu, Au and Mn have had economic importance, as El Indio district (Au-Cu-As) in the headwaters of Toro River, (Jannas et al., 1999). Several studies analysis the relation between the mineralization and alteration of the rocks surface in the drainage basin, principally during episodes related to flood episodes events (Oyarzún et al., 2012), where the contamination to the river introduce an environmental problem. According to Oyarzún et al., (2003; 2013) elements like As, Cu, and Zn is present with high levels, next to Mn, Fe, and Al in Elqui and their tributaries rivers. The surface values vary significantly seasonally with a minimum in summer and maximum in winter, in contrast, groundwaters show only moderate seasonal change. These elements are provided by El Indio district that geological characteristic permit the acid drainage generation, sulfide-rich mineralogy, advance argillic alteration zones, and facture rock allow the infiltration in the groundwater to the principal channel.

The Claro and Turbio River's presents steep longitudinal profiles and very narrow alluvial plains. In contrast, to the Elqui River plain that have terraces close to Vicuña town. The Toro River is a glacio-fluvial valley filled by ancient glacio-fluvial sediments and modern colluvial sediments. La Laguna River is over a glacial valley with a glaciogenic and glacial deposits fills (Figure 1.3). Two sites exposing moraine system associated with ancient glacial margins are presents along the valley (Riquelme et al., 2012). The first site is located ~8 km downstream from Cerro El Tapado at 3700 masl and comprise a single frontal moraine reaching more than 50 m above the current's river floor valley. The second site is located farther downstream at La Laguna (3150 masl) and comprises three lateral moraine arches.

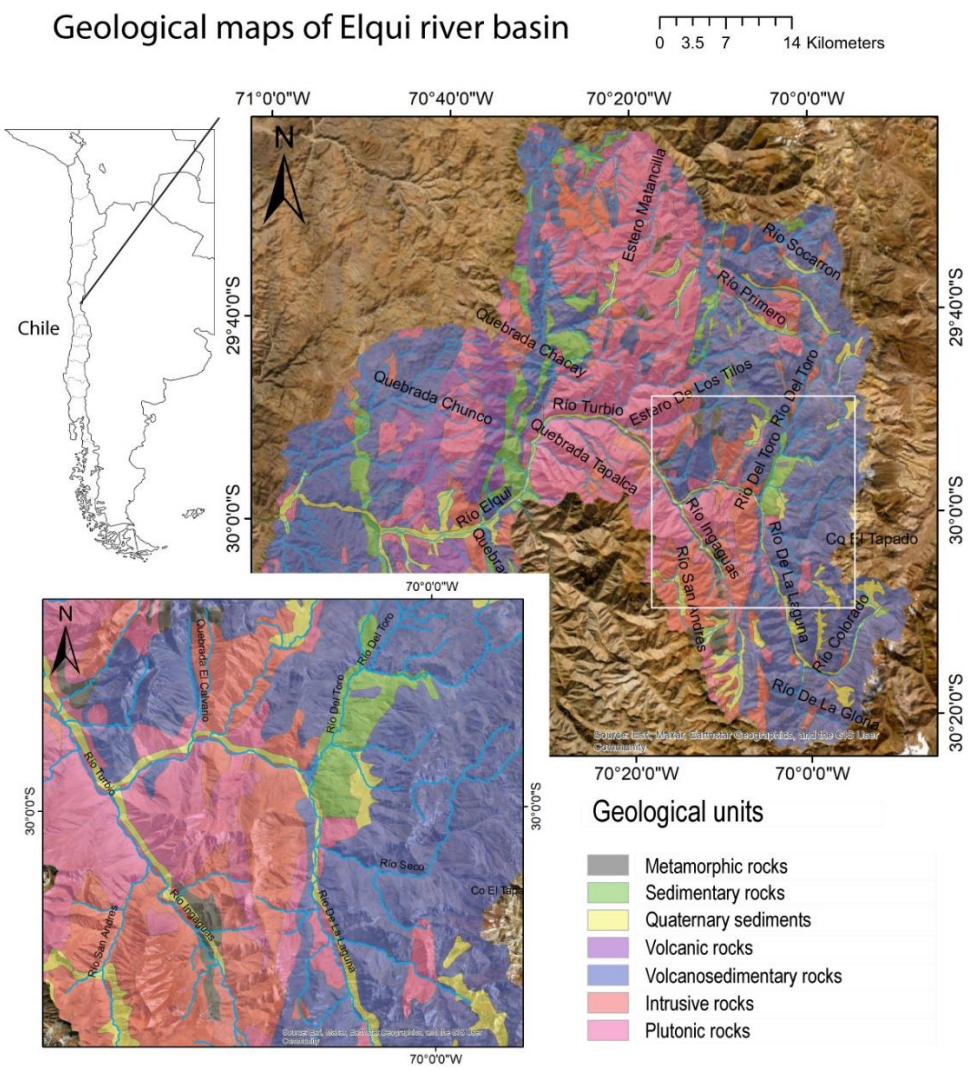

Figure 1.3. Synthetized geological map units according to their principal lithology in the surface basin.

1.2 Modern and Holocene Climate in semiarid region

The study area corresponds to the Chilean Andean Mountain territory of the Coquimbo region, which is in the Central North or semi-arid sub-region climatic zones (Lat. 29°S to 32°S). Coquimbo region is a transitional zone between the arid Atacama region and Mediterranean climate of central Chile. The main climate elements in the region are determined by the combined effects of oceanographic, atmospheric, and orographic factors.

In front of Chilean margin, the South Pacific Subtropical High (SPSH) a semi-permanent system of high pressure, changes seasonal from 35°S, 90°W in January to 25°S, 90°W in July. During the northward seasonally migration of SPSA, westerlies (SWW) carrying frontal systems expand equatorward to about 30°S (Garreaud et al., 2009) concentrating the rainy season between July and August during the austral winter. The clime is also influenced by superimposed oceanic and atmospheric phenomena such as the

Niño/Southern Oscillation (ENSO) and Pacific Decadal Oscillation (PDO) (Aceituno, 1988; Rutllant and Fuenzalida, 1991; Montecinos and Aceituno, 2003).

However, current climatic situation has not been constant during the last 15000 years. Several paleoclimatic reconstruction studies that covering the longer chilean margin where SPA influence, suggest humid to dry climatic scenarios development during late Pleistocene to Holocene period. Climatic record, using lacustrine cores in Laguna Cerritos Blancos and Laguna El Cepo in Andean semi-arid region (Tiner et al., 2018), suggest that the Holocene began with wet period from 10800 to 9500 cal yr BP. A transition to dry conditions is from 9500 to 5500 cal yr BP, that is interrupted by stormy conditions from 8300 to 7600 cal yr BP. Wetter conditions prevailed from 5500 to 4100 cal yr BP, after a shortly dry period established during 4100 to 2200 cal yr BP. After 2200 cal yr BP, moisture increased until 500 cal yr BP when it began decreasing again into the present. In Río Turbio Valley Riquelme et al., (2011) interpreted two distinct episodes during the Holocene: First episode documented in fine grained sediment with early Holocene age (~11550 – 7800 cal ys BP) indicative of a dry climate; and a second period after that (~ 7800 or 5500 cal yr BP) interpreted as increase in the fluvial transport reflects wetter condition. Several paleoclimatic reconstruction research in Andean north of Chile and south of Perú, indicate that during the middle Holocene the cycles of ENOS was intensify (e.g., Vargas et al., 2013).

1.3 Climate and Sedimentary Processes

The climate drives the precipitation, temperature, humidity, wind, and anothers, that influence in the physical and chemical weathering conditioning the generation of sediment, but also may be control the rate of erosion, transport, and deposition in the different environment. For example, extreme rainfall event in arid to semi-arid region may produce landslide from the coastal to the Andean Mountain. In glacier environment, retreat of glaciers produces more sediments to the fluvial system and increase the stream flow and rise the sediment transport, in contrast the advance will lead to a decrease in sediments and its transport, resulting in the accumulation of then. In periglacial environment, where periods of snowfall are followed by periods with temperatures above 0°C, melting snow and permafrost can also produce landslides, and also may produces increase in the stream flow. Both situations generated an excess of runoff, erosive increase, and modification of the depositional process. Thus, the intensity of sedimentary processes (erosion, transport and sedimentation) is controlled by the climatic conditions of the environment. The accumulation of sediments reflects variations in sedimentary processes, as well as the environment through which they were transported, while the surfaces separating the sediment layers can indicate abrupt changes in environmental conditions, such as excess erosion, flooding, increase/decrease of water, among others.

Chronicles and monthly observational rainfall data analyzed since 1900, in the Coquimbo and Atacama regions of Chile (Ortega et al., 2019) support that the interplay between the

warm phases of ENSO and PDO modulate the frequency of the heaviest rainfall events in the southern edge of Atacama region, which have resulted in heavy rainfalls driving flood and debris/mud flow events during the second half of 20th century. On the other hand, in high-mountain periglacial environments landslides or debris flow also can be triggered by melting of the snow cover as well as of the interstitial ice of the active layer (Zischg et al., 2011). For example, 14% of the debris flows and rockfalls within Aconcagua Park (Argentine Central Andes) are triggered by snowmelt and are likely to be higher in the spring and summer after El Niño winters (Moreiras et al., 2012). Similarly, in the Chilean semi-arid Andes, debris flows were studied and suggest melt water triggered (Vergara Dal Pont et al., 2019). This indicates that sedimentary processes are being affected by the current extreme climatic conditions, which are producing short-term changes in the mountain systems, and it is necessary to know what the conditions were like in the past in order to elucidate the future effects.

2 METHODS

Five sites (Figure 1.2) were studied during a 12-day campaign in November (2019), January (2021) and October (2021). Sedimentological and stratigraphic characteristics, contact and spatial arrangement between stratigraphic units, were detailed recognized and described, through the elaboration of stratigraphic columns and profiles at 1:100 scale. The outcrops successions were continuously sampled at 20 to 50 cm intervals approximately considering changes in grain size, color, or grain composition, for sedimentological and geochemistry analyses.

2.1 Stratigraphy, sedimentary facies, and architectural elements analysis

Six stratigraphic profiles were measured at a metrical scale on five outcrop sections (Figure 1.2). The sediment and associated sedimentary structure are easily documented during the fieldwork due to good exposition of the slope deposit.

Facies was defined during the sedimentological analysis using statistical grain-size results, such as type of sediment, proportion of mud, mean, mode, and sorting, and stratigraphic features, then was contrasting with the alluvial facies proposed by Miall (1996). Subsequently Architectural Elements (AE) were develop based on field observation and photography of the section analysis of the alluvial deposits outcrops and was linked with the Facies Association (FA). In this way, the surface, and their order, together with the geometry, size and arrangement of the internal layers allow to define the AE, which are well documented by Miall (2013, 2020). Using stratigraphic, facies and AE data, allow to interpret the FA being a good parameter to understand the sedimentary processes and paleoenvironment system.

2.2 Grain-size analysis

Forty sediment samples were selected for detailed grain size analysis corresponding to five sites in the Río Turbio Valley (Figure 1.2).

The grain size weight percentages were obtained by laser diffraction methods using a Mastersizer 2000 (Malvern Instruments Limited, Malvern, UK). This analysis and sample preparation were performed in the Department of Geology at the Universidad de Chile. The samples were sieved (No. 18) for obtain particles size fraction finer than 1 mm.

The results of the grain-size distributions were statistically studied using the graphical and moments method calculated using Gradistat (Folk and Ward, 1957). The grain size distribution was represented in a frequency curve. Through the method of moments four statistical parameter were measured: (a) mean; (b) sorting; (c) skewness that is a measure of symmetry of the grain-size distribution curve; and (d) kurtosis.

2.3 Energy dispersive X-Ray Fluorescence (EDXRF)

EDXRF analyses were carried out at sedimentary strata variation using an EDX-720 Shimadzu spectrometer at the X-Ray Fluorescence Laboratory in the Department of Geology at the Universidad de Chile. The XRF spectrometer was operated using an Rh X-ray tube set to 15–50 kV and 1000 μA. EDXRF analysis offers a quick, non-destructive, multi elemental method for determining major element composition (from Na (z = 11) to U (z = 92)).

A total of n = 27 samples were analyzed, 10 belonging to core Southwest Slope deposits (SWS), and 17 from Northwest Slope deposits (NWS). Prior to analysis, each sample was homogenized and grounded with an agate mortar and pestle.

2.4 Radiocarbon dating

A total of 6 samples were collected in layers with organic matter for 14C radiocarbon dating by accelerator mass spectrometry (AMS). All samples were analyzed in the DirectAMS laboratory, USA. Calibrated radiocarbon ages were determined using SHcal20 calibration curve (Hoggs et al., 2020) in Calib program (Stuiver et al., 1993).

3 RESULTS

3.1 Stratigraphic and sedimentological analysis

The sedimentological study involved the analyses of grain size results and the stratigraphy and sedimentology field observations, at sedimentary successions from 5 outcrop deposits studied (Figure 1.2). The sediments were classified using Folk & Ward, 1974 granulometric classification, which then were grouped in four main sediment types: gravels, sands, silts, and clays. The stratigraphy analysis used to identify the geometry of the sedimentary units, their vertical and lateral distribution, and the stratigraphic surface. The statistical analyses of grain size sediment permit us obtaining the average diameter and mode of each sedimentary facies, and the degree of sorting of the sediment. The joint analysis of sedimentology and stratigraphy allow us: (1) to define the sedimentary facies and (2) to observe the stratigraphic patterns for the interpretation of the facies associations that will be discussed later. The samples, facies, and sedimentology of the sediment in

each outcrop is summarized in supplementary material (**¡Error! No se encuentra el origen de la referencia.**).

3.1.1 Sedimentary facies

The sedimentary facies defined in the Río Turbio valley deposits, located between ravine El Calvario and Piuquenes (Figure 1.2), are classified into three major facies: Conglomeratic facies (Gcm, Gt, Gp, Gmg and Gmm), Sandstone facies (Sp, St, and Sr), Fine-grained facies (Fl, Fr) and Biogenetic facies (C). Each group of facies was defined based on the elements they shared, such as grain size, sedimentary properties, sedimentary structures, and stratification surfaces. The grain size distribution curves of each group of facies (Figure **3.4**) allow visualizing the homogeneous or heterogeneous grain-size tendency of the sediment, as well as the representative grain size of each facies group. The sedimentological and stratigraphic characteristics of each sedimentary facies are defined and described below. These groups are constituted by two or more facies identified using the facies classification from Miall, (1996).

Table 3.1. Facies described and they principal sedimentary feature and interpretation by Miall (1996).

Facies (Miall, 1996)	Lithology	Sedimentology	Sedimentary structures	Interpretation (Miall, 1996)
Gcm	Clast-supported conglomerate	Moderately sorted and unimodal sand to muddy sand matrix.	Massive	Gravel channel lags
Gt			Through crossbedding	Accretional lateral gravel-bars
Gp			Planar crossbedding	Transverse to lateral gravel-bars
Gmg	Matrix-supported conglomerate	Poorly sorted and unimodal to bimodal muddy sand matrix	Inverse to normal grading	Pseudoplastic debris flow (low strength, viscous)
Gmm			Weak grading, massive	Plastic debris flow (high-strength, viscous)
Sp	Coarse to very coarse sandstone	Moderately to poorly sorted and unimodal to bimodal fine sand matrix.	Planar crossbedding	Lateral sandbars
St			Trough crossbedding	Accretional lateral sandbars
Sr	Very fine to fine sandstone	Moderately to poorly sorted and unimodal fine to very fine sands	wavy and lenticular lamination, climbing ripples	Current ripples in a moderated regime to the dense flow
Fl	Silts	Poorly to very poorly sorted and unimodal very coarse silt	Ripples and planar lamination, trough cross stratification or massive	Distal waning flood deposits
Fr	Muds	Poorly to moderately sorted and unimodal very coarse silt.	Massive and locally difusse parallel wavy to planar lamination.	Decantation processes in a stagnant water

C (Cm-Om)	Coal mud	Poorly to very poorly sorted unimodal to bimodal coars silts	Plant macrorest, mud laminae	Incipient soil

3.1.1.1 Conglomeratic facies

Conglomeratic facies contain a significant proportion of pebble-size and largest clast with a fine to medium sandy matrix (Figure 3.4. A) and it divided into matrix-supported (Facies-A) and clast-supported (Facies-B). Each one is subdivided into five lithofacies according to Miall 1996 (Gcm, Gt, Gp, Gmg and Gmm).

Facies-A (Clast-supported gravels)

Description: These facies comprises a semi consolidated clasts-supported pebble to cobble, subangular to surround, polymictic well sorted gravels. The gravels composition are a volcanics and less intrusive lithics, their shapes vary from spheric to oblate, and clast-sizes ranging from pebbles to cobble (2-35 cm). The matrix is composed by sand to muddy sand size, are moderately sorted, with a unimodal distribution graph, their medium grain-size is fine sand, and the mud contents if of 0.1% to 65% (Tabla 2). These facies shown two difference aspect identified according to their sedimentary structure such Miall (1996) classification facies: Massive (Gcm); trough crossbedding (Gt), and tabular crossbedding (Gp) (Figure 3.1. A; D; E).

Interpretation: Clast supported, sorted gravels, sand matrix and gravels shape, indicate a long transport period of the sediment, in a turbulent-high energy regimen flow, that had a sufficient energy and time to generate a subrounder, spheric and oblate shape clasts. Gravels with trough (Gt) and planar crossbedding (Gp), represent the juxtaposition of inclined layers originated by the migration of longitudinal and transversal bars. Massive clasts supported gravels (Gcm) represent gravels lags channel deposited during a high-energy discharge episode, with the subsequent establishment to the normal flow.

Facies-B (Matrix supported gravels)

Description: This facies comprises a semi consolidated matrix supported granule to pebble, angular to subangular, polymictic moderately sorted gravels. The gravels composition is volcanics and less intrusive lithics, their shapes vary from spheric to oblate, and clast-sizes ranging from granule to pebble (2-6 cm). The matrix is sand to muddy sand size, poorly sorted, with a unimodal distribution graph, the medium grain-size is medium to coarse sand, and the mud content is from 65 to 0.1% clay (Tabla 2). These facies shown two difference aspect identified according to the sedimentary structure such Miall (1996) classification facies: imbricated with inverse to normal grading (Gmg) or massive gravels (Gmm). The gravels are interbedding with lenticular sand body with planar cross stratification (Figure 3.1. B; C; F).

Interpretation: The gravels grain size and texture (matrix supported, poorly sorted conglomerate) with a muddy sand matrix indicate a turbulent, high-energy, high-density flow, also represent a short period of transport, by traction and suspension, including the suspension by floatability of gravel inside a muddy matrix. Normal gradation gravels refer to a density current to experience a deceleration in their velocity, while inverse gradation occurs by destabilization of high gradient zone, where successive waves of debris flows occur. The inertial forces operating in these flows transport large blocks by gravity sliding, rollover or saltation, which are accumulated by granular impact in areas of slope change granular impact in areas of slope change (Nemec, 1990).

3.1.1.2 Sandstone facies

Facies Sp and St (coarse to very coarse sands planar cross-bedding (Sp) and trough cross lamination (St))

Description: This facies comprises an unconsolidated matrix supported by granule to coarse sands, subangular and angular, polymictic, poorly sorted sandy conglomerate. The gravels size composition is volcanics and less intrusive lithics, their shapes vary from spherical to sub-prismatic, and clast-sizes is granule (~1-2 cm). The matrix is sands to muddy sand matrix, poorly sorted, with an unimodal to bimodal distribution graph, the medium grain-size is medium to fine sand, and the mud content is from 40 to 0.4%. Large planar (Sp) and trough (St) cross stratification have been identified, in addition abundant Ryzolites characterized the sediment (Figure 3.2. A, B y C). The internal strata contain fine gravels layers oriented to stratification, gravels clusters, and mud laminations.

Interpretation: Large planar and trough cross stratification over an irregular and net surface, suggest the development and accretion to the lateral sand's bars. Rhyzolite trace, that cut stratification, involved the subaerial bars exposure during a period of lower fluvial flow.

Facies Sr (Very fine to fine sands ripples)

Description: This facies comprises a semi consolidate fine sands to silty sands, moderately to poorly sorted. The granulometric distribution indicate an unimodal to bimodal graph, the medium grain-size is fine to very fine sands, and to mud content is from 60 to 5%. The sands present trough cross lamination, climbing ripples, and deformation structures (Figure 3.2. D), locally present wavy lamination and Ryzolites in stratigraphic surface over fine grain facies (Figure 3.2. E). Euhedral crystal gypsum in a sandy matrix is locally observed as planar stratum, with prismatic to rosette crystals shape. Local laminate of organic matter as coal is identify.

Interpretation: Grain size indicated a moderated energy flow regime in subaqueous medium such as ripples current represents. The cross lamination and climbing ripples indicated a unidirectional flow, the last indicate the traction and decantation transport type associated to and dense moderate energy flow, which is consistent with the large

proportion of clays (60%). Wavy lamination to the top indicate variation of energy condition, to a low energy flow. The local gypsum sandy matrix is interpreted as evaporation rise allow the precipitation of gypsum as euhedral crystal.

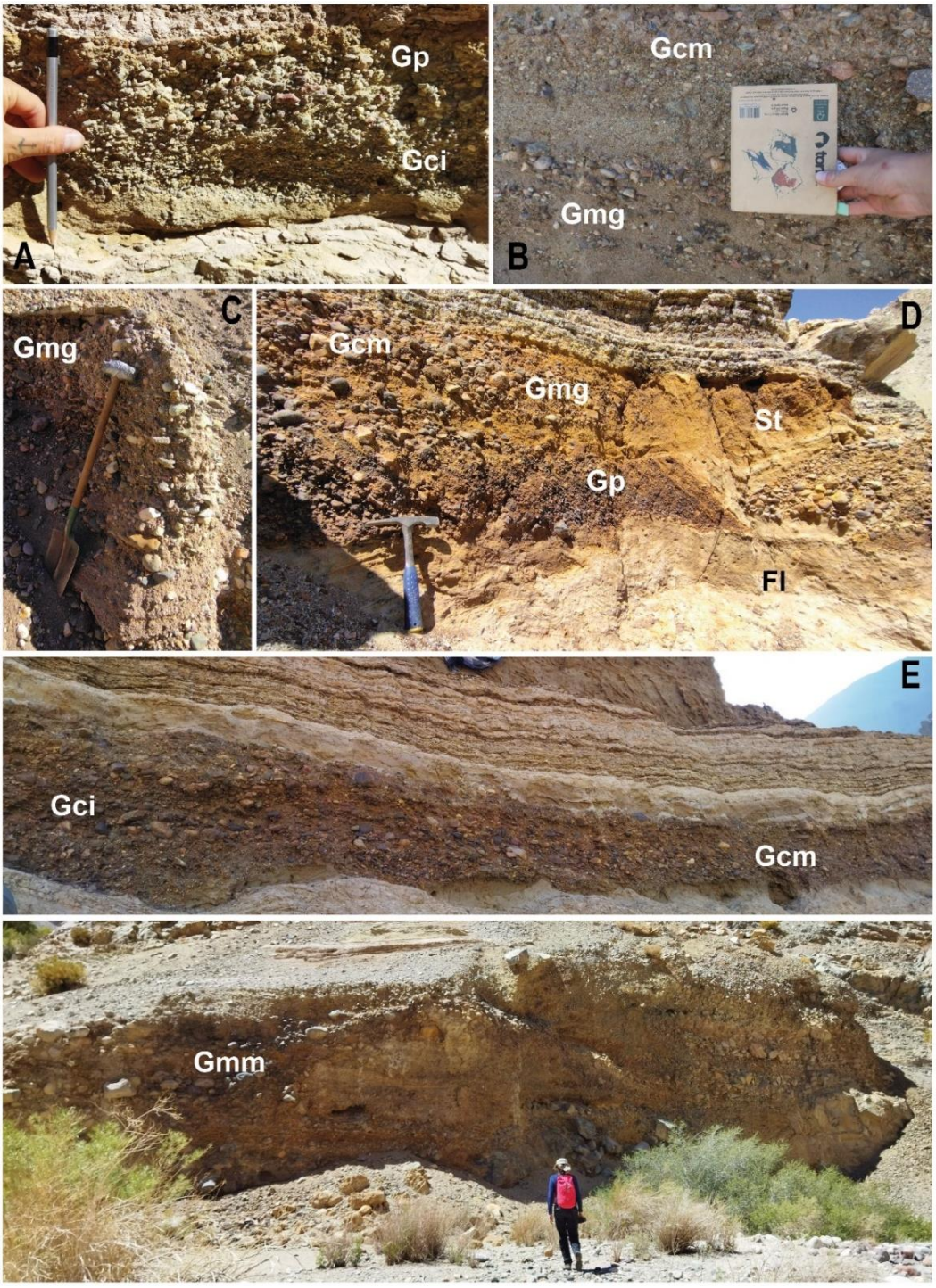

Figure 3.1. Photographs of conglomeratic facies in the study sites. A: SES; B: SWS; D: NES; E: SWS and F: NWS.

3.1.1.3 Fine-grained facies

Facies Fl (Siltstone with planar and ripples lamination)

Description: This facies comprises a semi consolidate poorly to moderately sorted muddy sand. The granulometric distribution indicate an unimodal to bimodal graph, the medium grain-size is very fine sand to very coarse to coarse silt, and the mud content is above 20%. Mainly presents ripples, trough cross stratification, sub-horizontal parallel lamination, or massive silts, and locally presents lens or lamination of muds (Figure 3.3. F). Ryzolites, organic matter, gypsum within a lime matrix and iron oxides minerals is observed subordinate. Internal gradually of coarsening upward from clay to silt sediments it is usual. Locally laminated sands to the top are observed.

Interpretation: Fine grain sediment (silts) were transported as suspension in a subaqueous medium, trough cross stratification indicates migration of ripples bedform under an unidirectional flow. Parallel lamination, massive silts and local lenticular muds represents lower energy state. Rhizolites and organic matter accumulation likely is associated to the water stagnation and pedogenetic processes during a subaerial exposed. The development of coal occurs when the organic matter accumulation is covering by a dense current.

Facies Fr (Massive mudstone)

Description: This facies comprises a well consolidated poorly sorted to moderately sorted sandy mud. Granulometric distribution show unimodal to bimodal graph, the medium grain-size is very coarse to very coarse silt, and the mud content is above 20% to 85%. This facies presents mostly massive mud stratum, and in some case with diffuse ripples and planar laminations, or deformation structures in contact, and locally sands lamination. Rhizolites, wood debris, disseminated organic matter, and stratum with gypsum as euhedral crystal of different sizes with a limes matrix are observed (Figure 3.3).

Interpretation: These facies are representative by massive to subhorizontal lamination clays, this is indicative to the suspension transport and decantation sedimentation in a lower energy regime condition. Symmetrical wavy laminations indicate local oscillatory wave under a water carpet, locally sands laminates likely represent a discharge period that give the organic matter. Gypsum formed under an evaporation process likely to large insolation period.

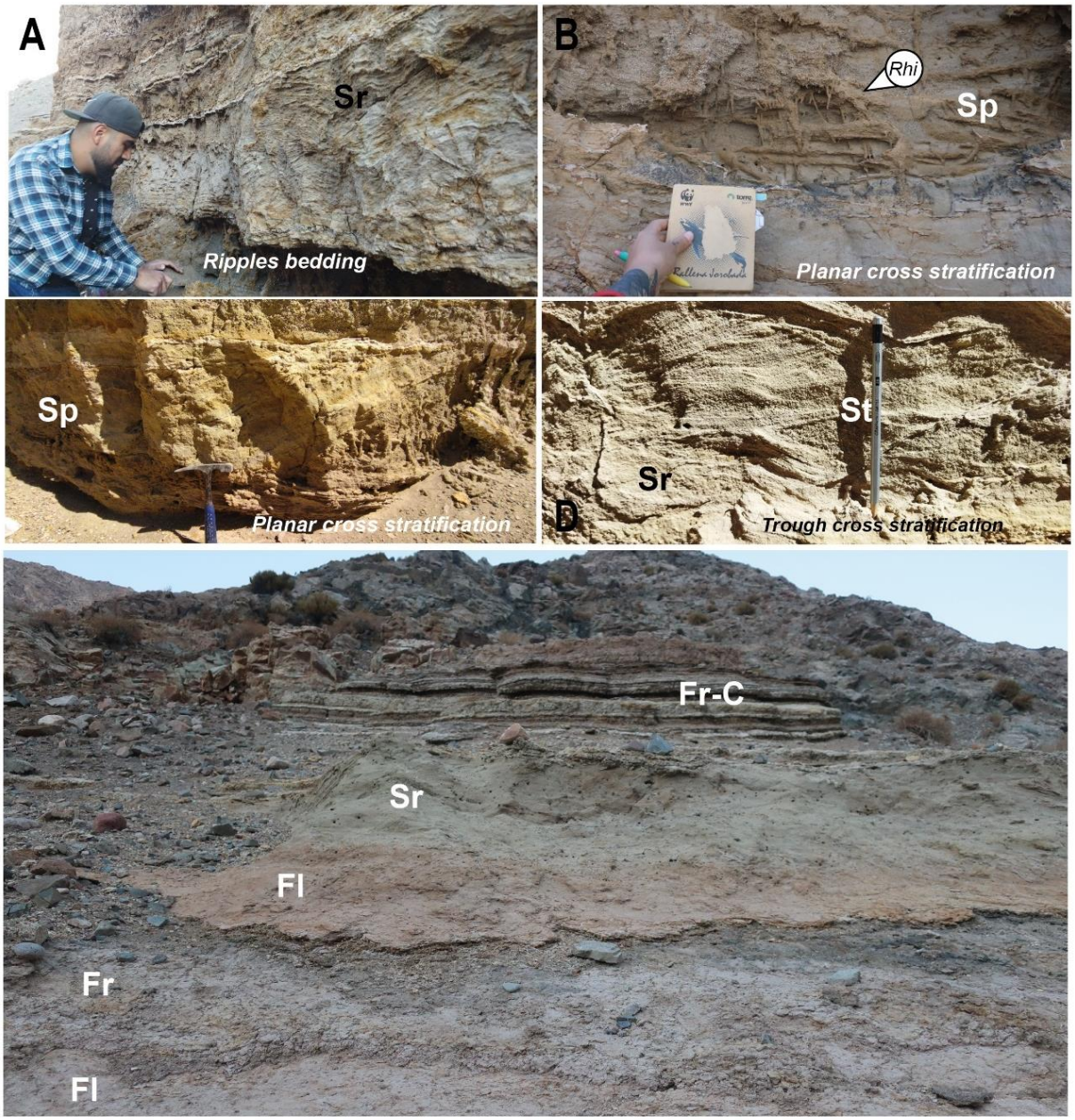

Figure 3.2. Photographs of sandstone facies in the study sites. A: SWS; B: SWS; C: SES; E: SWS; F: SES and G: NWS

3.1.1.4 Biochemical sediment facies

Facies C

Description: This facies comprises a well consolidated to semi consolidated Intercalations of muddy sand, gypsum muddy matrix, and muddy sand beds with laminated of organic matter, Ox Mn and Ox Fe layers. The distribution grain-size graph is unimodal to bimodal, indicate that sediment is poorly to very poorly sorted, their medium grain-size is coarse to very coarse silt, and mud content is above 50%. Rhizolites abundant, and massive, planar and wavy parallel lamination dominate the sedimentary structures, locally may be present

planar and trough cross stratification. When these facies are underlying sand facies (Sf and Sc facies) or when clay are in contact with fine sands lenses on the bottom, usually contacts present chaotic structures, (Figure 3.3).

Interpretation: The transport is interpreted as suspension and decantation process sedimentation; wavy lamination indicates a bidirectional lower flow regime and though cross lamination unidirectional moderated flow regime.

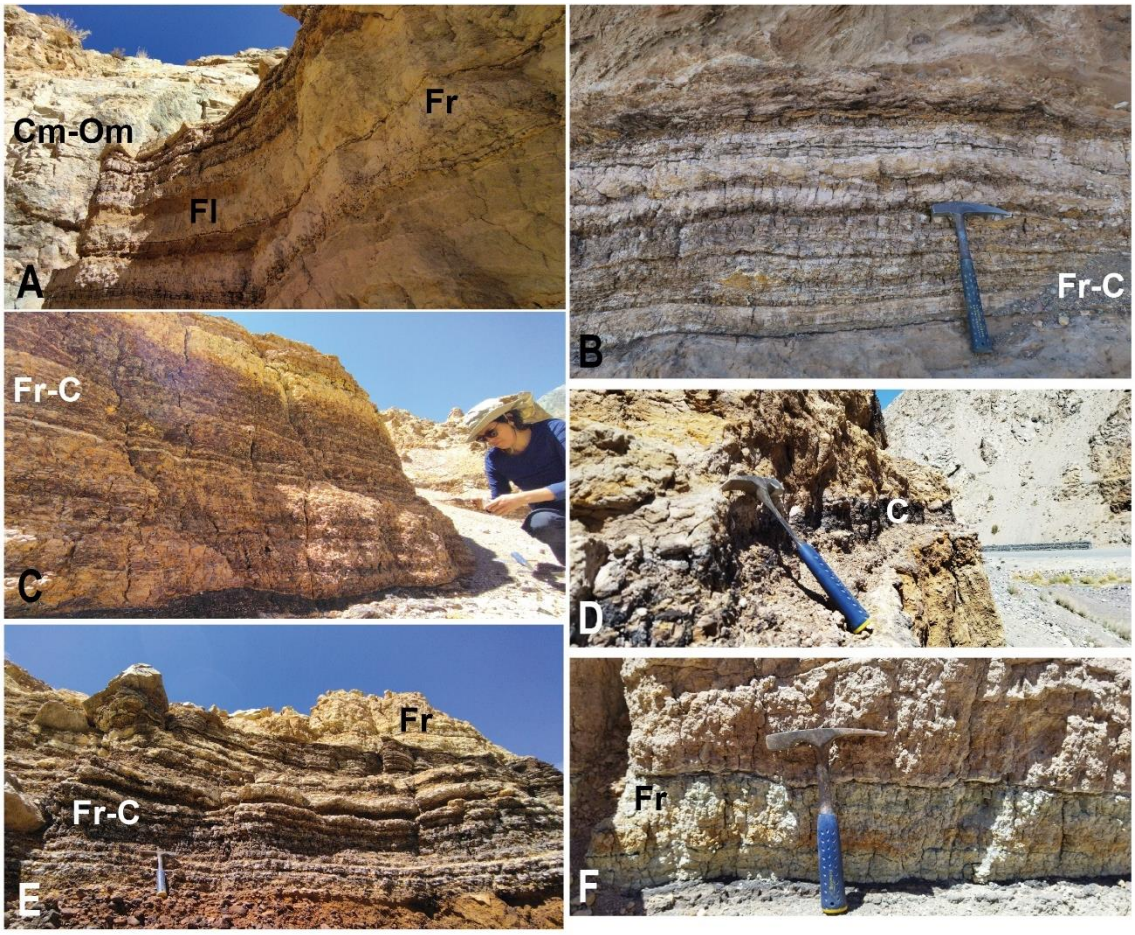

Figure 3.3. Photographs of fine-grained and biochemical facies in the study sites. A: SES; B: SWS; C: EL Calvari; D: NES; F: NES; E: El Calvario, high part.

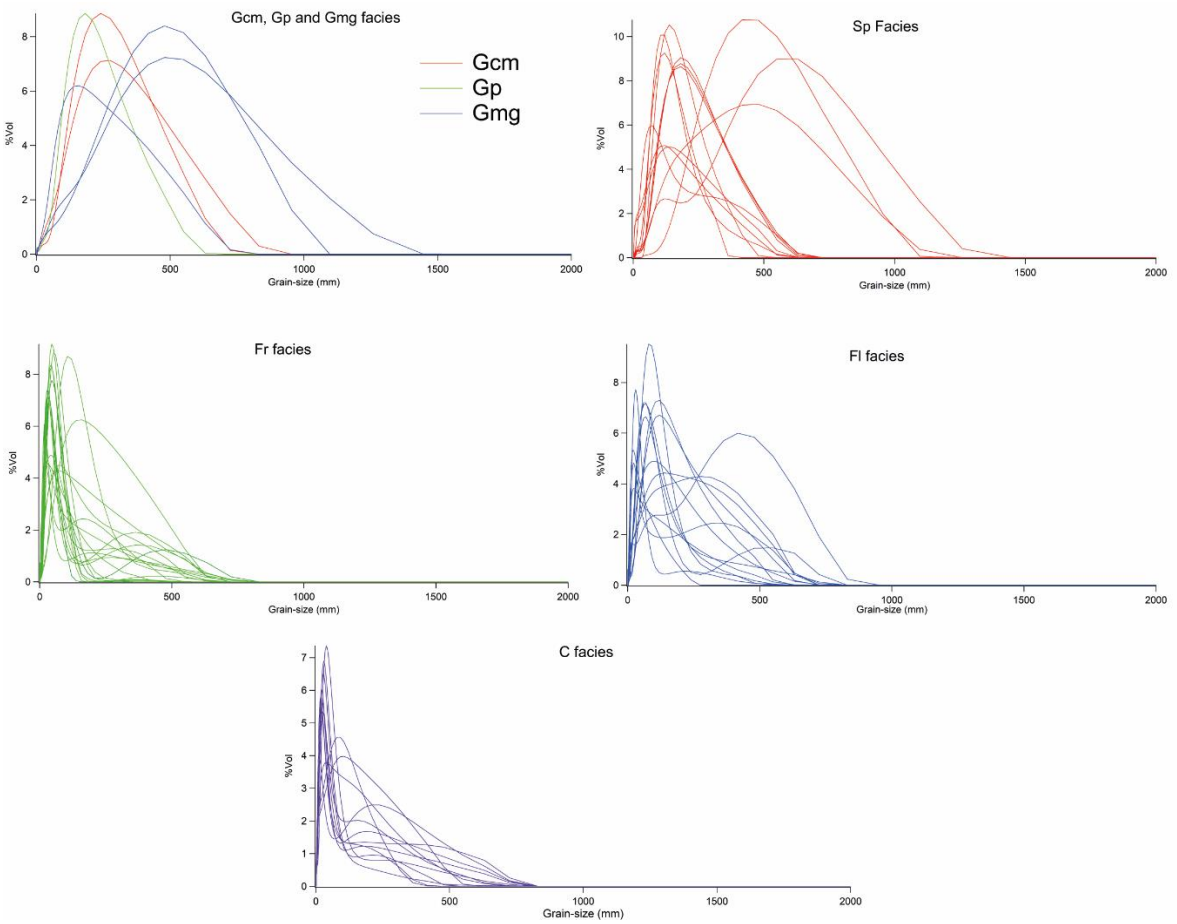

Figure 3.4. Grain-size distribution graphic of each sedimentary facies. The tendency to decrease the grain size from the gravelly facies (Gcm, Gp, Gmg) to those sandy (Sp) or muddy (Fr, Fl, C) facies can be observed.

3.1.2 Stratigraphic successions

The vertical and lateral stratigraphic distribution of the sedimentary facies permit us visualize the vertical facies association and geometry of the deposits at the Turbio Valley (Figure 1.2). In the followed section is described the stratigraphy of the Turbio valley sedimentary succession.

3.1.2.1 Stratigraphic succession of Southwest Slope deposits (SWS)

SWS is in the south slope of the valley (Figure 1.2). Two columns were constructed (Figure 3.5) separated with each other 4 to 5 m and represents the first 10 meters of the Southwest slope deposits (Figure 3.5)

The column (A) comprises a heterogeneous and cyclic vertical stratigraphic architecture (Figure 3.5). First four meters consist in a set of tabular layers in a vertical succession from fine grain facies (Fr-Fl) to sandstone facies (Sr, Sp) that repeats itself towards the ceiling. Local biological facies layer and gypsum interbed with fine-grains facies layers. In the middle (3.4 to 5.2 m) a large bedform with a grooved base are in contact with sandstones in an irregular and chaotic contact. These facies exposed a lenticular

geometry, concave base with plane roof, laterally is wedge with sandstone facies (Figure 3.5). The sedimentary fill comprises Sp facies and Gc facies, in a metrical through crossbedding (Figure 3.5, C). The rest of the succession finally with the repeating of fining upward successions, conglomeratic (Gmg) to sandstones (Sr, Sp) and muddy facies (Fl, Fr, C) interbedding (Figure 3.5).

The column (B) (Figure 3.5) is observed as a cyclic and heterogeneous vertical stratigraphic architecture. The column starts with an unknow thickness of a conglomeratic facies layer (Gcm). Then, in a net and irregular contact, a fining upward succession from coarse sandstones facies (Sp) to fine sandstones (Sr) and muds (Fl-Fr) facies are superimposed (Figure 3.5). Close to the 3 m, a lenticular layer with conglomeratic facies (Gcm) which grades vertically from fine sandstones (Sr) to mudstones (Fr) interbedding with limestones (Fl). Over 4 m is superimposed two fining upward vertical facies succession, from coarse sandstones (Sp) to fine -sandstones and -grained facies. The rest of the succession finally with the repeating of fining upward successions, conglomeratic (Gmg) to sandstones (Sr, Sp) and muddy facies (Fl, Fr, C) interbedding. Locally, centimetric beds of biogenic sediment interbedding fine grained facies layers.

3.1.2.2 Stratigraphic succession of Southeast slope deposits (SES)

Stratigraphic succession of SES comprise a small deposit situated 800 m eastward SWS by the same slope. The stratigraphic column represents a heterolytic and fining upward succession of 6 m thickness (Figure 3.7). The first m of the column includes planar coarse sandstone (Sp) layer intercalation with laterally wedge conglomeratic (Gcm) strata (Figure 3.2. C-D). Above 1 meter an intercalation of fine sands and mud are planar interbedding until the 3 m. The rest of the succession finished with lamination of muddy facies (Fl, Fr) (Figure 3.3. A) with biogenetic and gypsum local laminates.

3.1.2.3 Stratigraphic succession of Northwest Slope deposits (NWS)

Stratigraphic succession of NWS deposits is located in the north slope of the valley, just 0.2 km in front SES (Figure 1.2). The stratigraphic column represents a heterogeneous fining upward succession (Figure 3.6). The succession starts with 4 m of irregular layer of conglomeratic facies (Gmm-Gcm) (Figure 3.1. F). Immediately above in an irregular-net contact is superimposed an intercalation sandstone (Sr), limestone (Fl) and mudstones (Fr) planar bed, util the 3 m (Figure 3.2. E). The column finishes with lamination muddy facies with laminates of biological sediment facies.

3.1.2.4 Stratigraphic succession of Northeast slope deposits (NES)

Stratigraphic succession of NES is located to 0.16 km western of NWS at the same slope valley (Figure 1.2). The stratigraphic column represents a heterogeneous fining upward succession, which the first meter includes planar beds of muddy facies (Fl-Fr) upgrading to fine sandstone facies (Sr) (Figure 3.3. D). From 1.5 to 4.8 m a fine upward stratification from conglomeratic facies (Gmg, Gcm) to fine -sandstone and -grained facies (Fr-Fl) succeeded the muddy facies. Over 4.8 in a net contact, an irregular bed, with concave

base of conglomeratic facies is observed up to 5.5 m (Figure 3.1. D). Planar strata of fine facies intercalation dominated the rest of the sequence with laminates of organic sediment (Figure 3.3. E; Figure 3.6)

3.1.2.5 Stratigraphic succession of El Calvario deposits

Stratigraphic succession of El Calvario deposits is located in front to the homonymous creek approximately 0.6 km from SWS (Figure 1.2). The column represents the first 7 m of the deposits, but the sediment extends more meters over the slope (e.g., Honores 2020). The vertical stratigraphy comprises a heterolytic and coarsening upward succession (Figure 3.7). An intercalation of fine grained (Fr, Fl) to sandstone facies strata comprises the first meter of the column (Figure 3.3. F), then a mud lamination (C-Fr-Fl) layer are superimposed in a planar-net contact until 3 m (Figure 3.3. C). The rest of the column finish with an interdigitation of gravel facies with fine facies strata ending by a thick irregular strata of gravel facies.

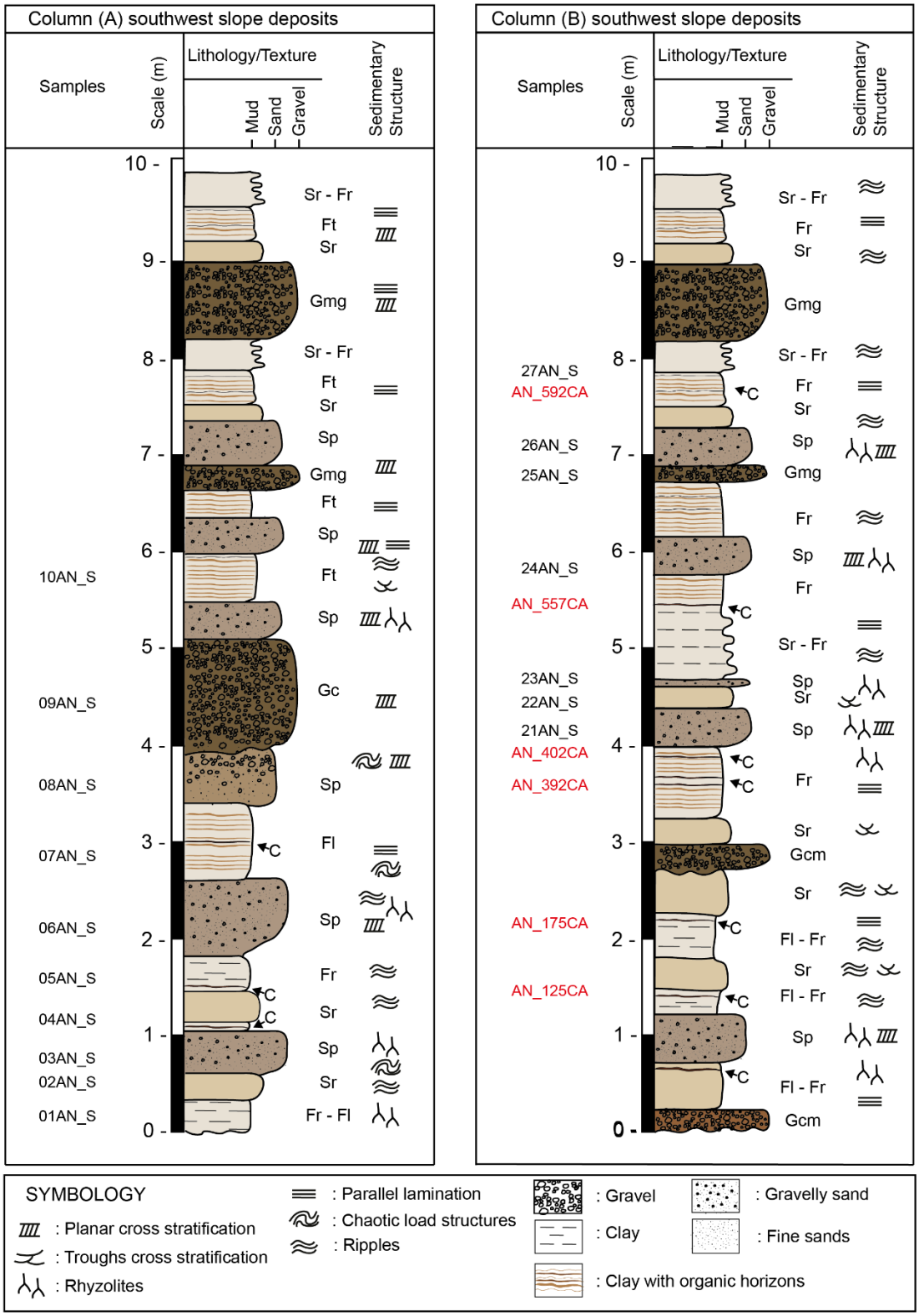

Figure 3.5. Southwest slope deposits

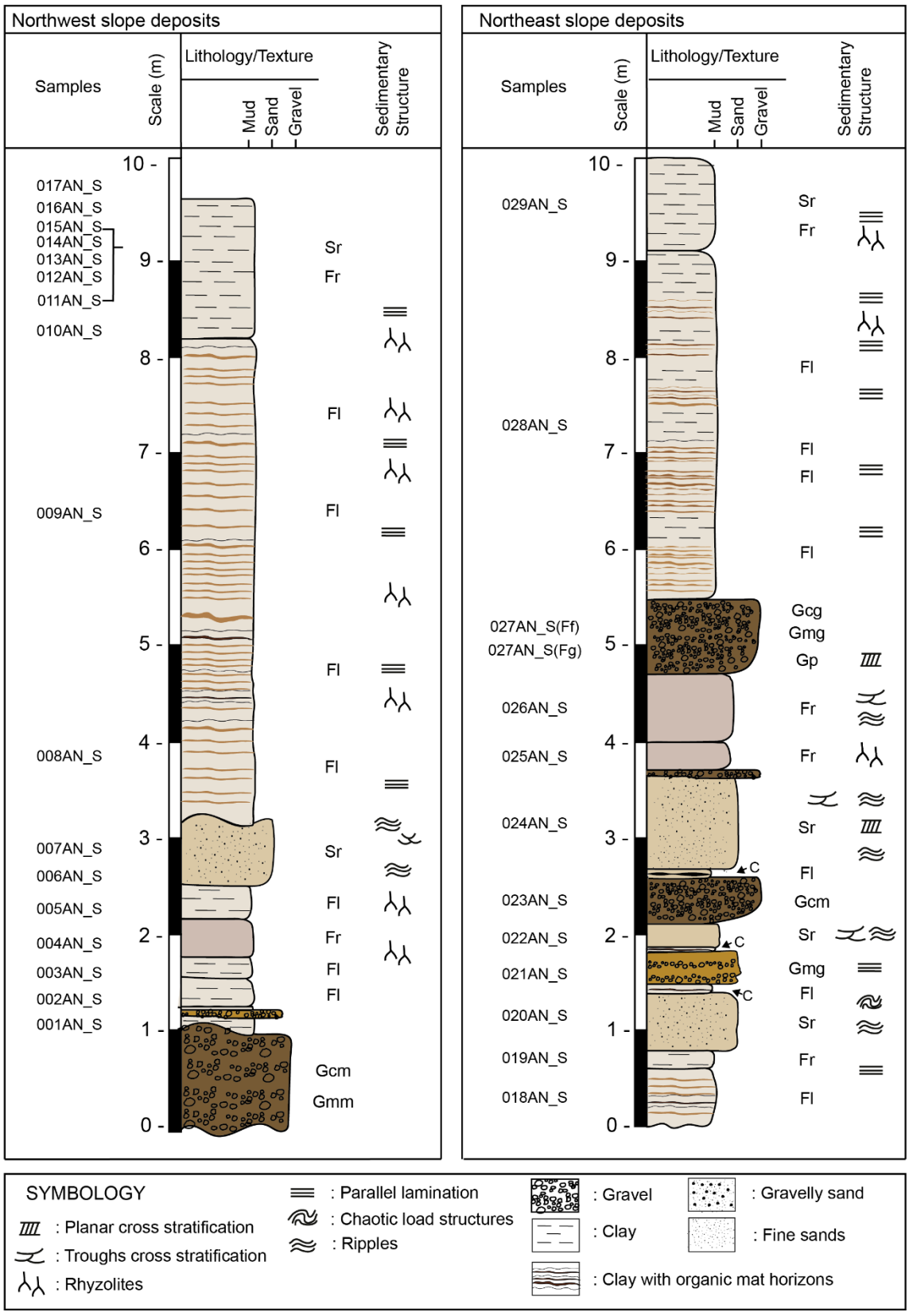

Figure 3.6. Stratigraphy of Northwest and Northeast slope deposits

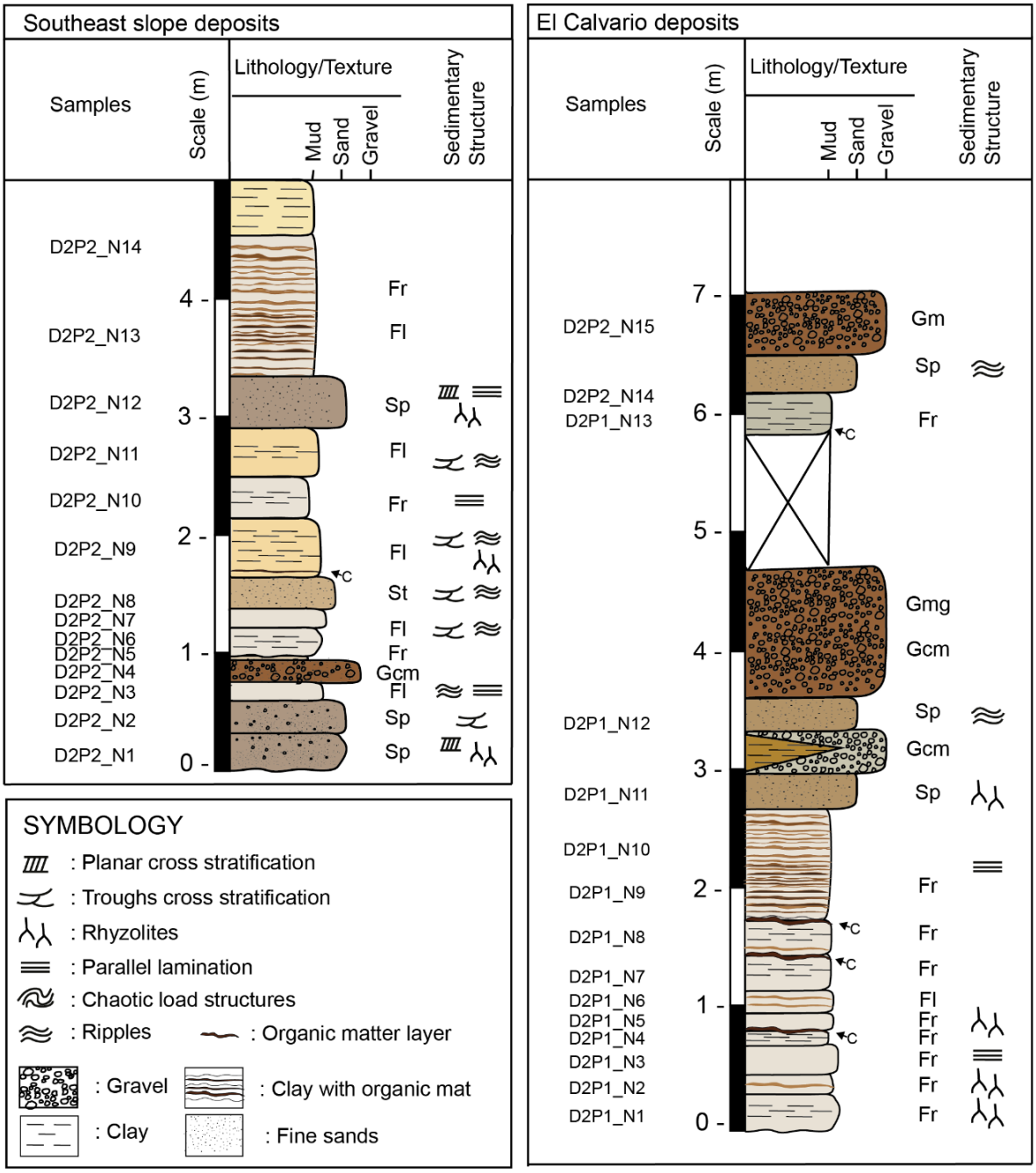

Figure 3.7. Stratigraphy of Southeast slope and El Calvario deposits

3.2 Inorganic geochemistry

Energy dispersive X-ray fluorescence (EDXRF) method were realized in sediment taken from fine-grained facies (3.1.1.3) in Northwest Slope (NWS) and Northeast Slope (NES) deposits (**Figure 1.2**), to obtain the concentration (Cps) of major inorganic elements.

About 15 chemical elements with the highest Cps values (counts per second) were measured, in which only 13 of them are available in all samples throughout the

sedimentary succession, these are Si, Al, Fe, K, Ca, S, Ti, Zn, Mn, Zr, Cu, Sr, and Rb. The elements that occur in higher proportions are Fe, Si, Zn, and Ti in both outcrops.

In the NWS outcrop, elements such as Si, Al, and K have vertically homogeneous concentrations. The highest values are associated with the more clayey and silty sediments, while a notable decrease in their values is observed in the sand-sized sediments. While Fe and S elements increase their concentrations in sandy sediments and decrease in muddy sediments. Elements such as Ca, Ti, Zn, Mn, Zr, Cu, Sr and Rb do not show a clear relationship with grain size. Among these elements, those more vertically homogeneous such as Zr and Ti and with a decreasing trend are observed, while Zn, Mn, Cu, Sr and Rb have a high vertical variability, with no apparent trend (Figure 3.8).

The sediments of the NES outcrop present different characteristics than the NWS sediments. The sandy sediments do not show a clear relationship with their elements, while the clayey sediments do and tend to have high concentrations of Si, Al, Fe, K, Ti, and Rb, and low concentrations of Ca, S, Zn, Mn, Cu, and Sr (Figure 3.9).

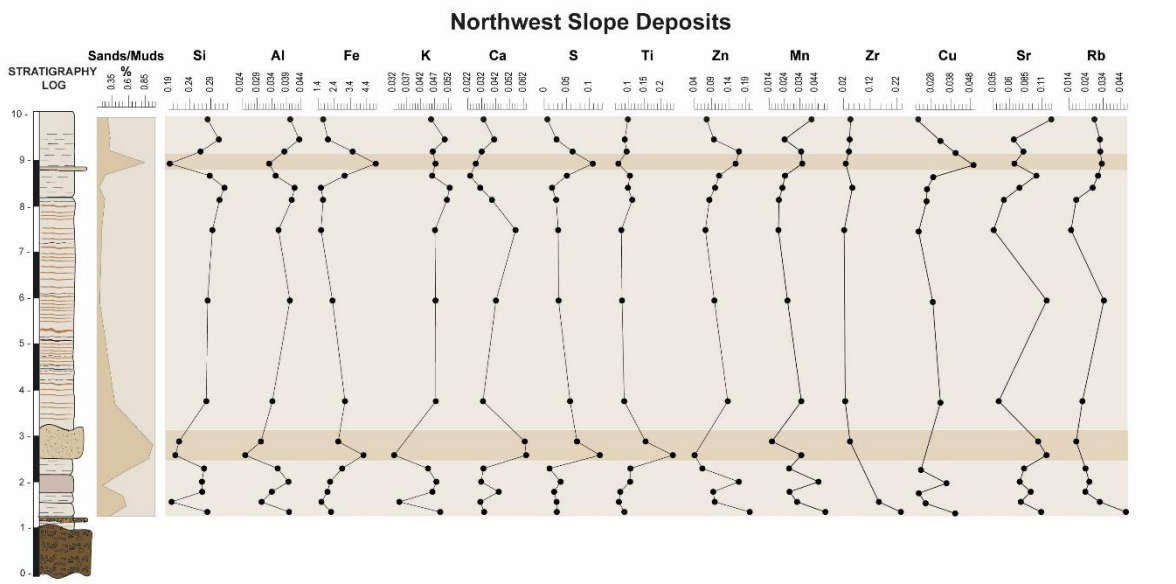

Figure 3.8. Major elements concentration variability on the vertical successions in NWS.

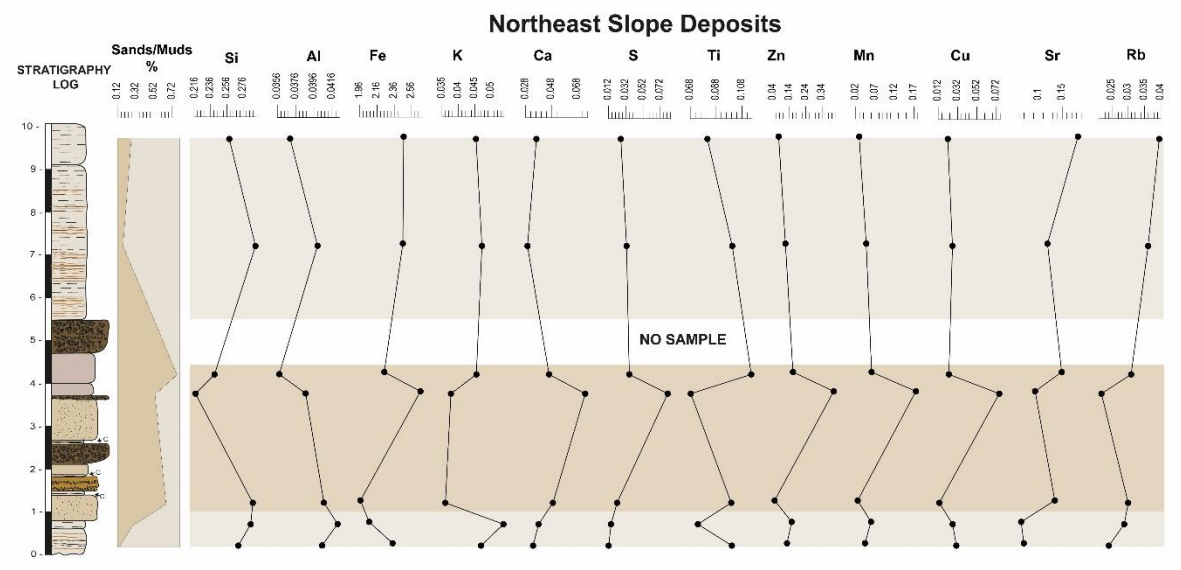

Figure 3.9. Major elements concentration variability on the vertical successions in NES.

3.3 Chronology

Six samples of organic matters in sediment were dating using the radiometric method C14. These samples were taken in mudstones that contain high organic matter concentration as laminates (Fr-facies) at the deposits of SWS location (Figure **3.5**). The summarized of age is in Table **3.2** and position on the outcrop is in Figure **3.10**. Also, it is used dating from previous work studies (Riquelme et al., 2011; Houbart, 2014; Honores 2021; and Calderon, 2021), the compilation is present in Table **3.2**. In work of Riquelme et al., (2011), the data correspond to layers from SWS and NES. While Houbart, (2014) and Honores (2021) presents ages from El Calvario deposits, and Calderon (2021), from the Huanta locality.

Table 3.2. Radiocarbon dates of Río Turbio valley succession obtain in this work.

Sample code	Method	Location	^{14}C yr BP	Age cal BP	Max age cal BP	Min age cal BP
AN_125CA	Radiocarbon	SWS	10011 ± 39	11309 ± 33	11276	11343
AN_175CA	Radiocarbon	SWS	9933 ± 44	11257 ± 18	11239	11276
AN_392CA	Radiocarbon	SWS	9744 ± 59	11120 ± 4	11116	11125
AN_402CA	Radiocarbon	SWS	9869 ± 38	11229 ± 14	11215	11243
AN_557CA	Radiocarbon	SWS	10055 ± 37	11384 ± 11	11373	11396
AN_592CA	Radiocarbon	SWS	9188 ± 35	10269 ± 28	10241	10297

* Calibrated calendar dates were obtained using curve SHCal 20 (Hogg et al., 2020), and the CALIB 810 program (Stuiver et al., 2021).

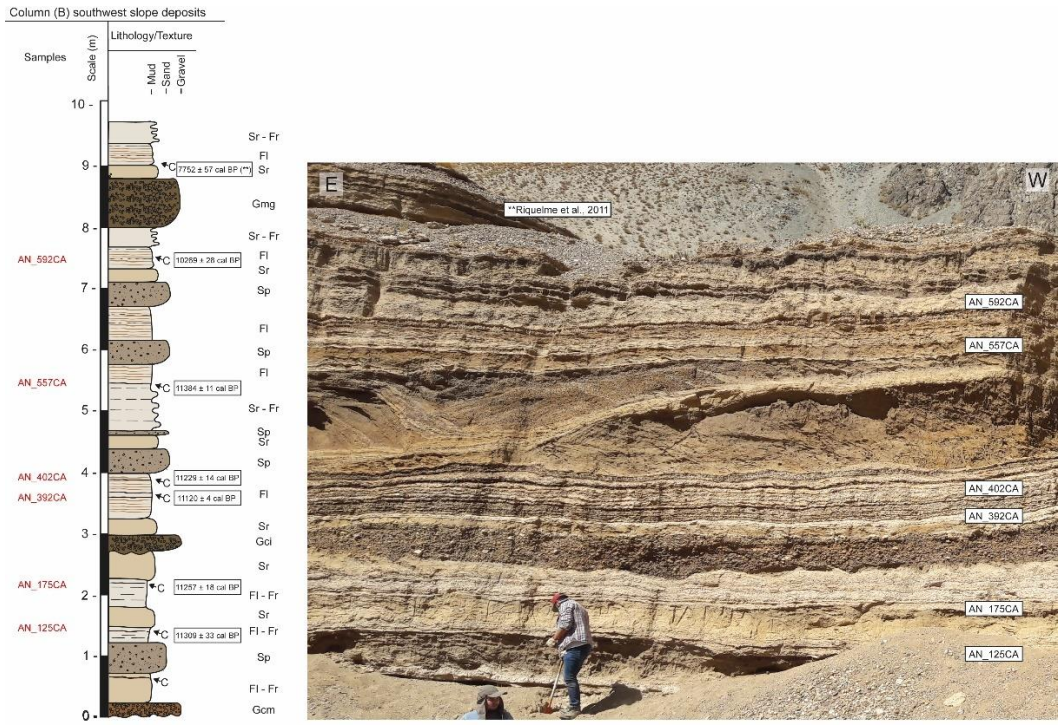

Figure 3.10. Radiocarbon dating results and position of the samples from SWS.

Table 3.3. Radiocarbon dates of Río Turbio valley succession compiled from previous works.

Sample code	Location	^{14}C yr BP	Age cal BP	Max age cal BP	Min age cal BP	Reference
EMOSITE1ECH2	Top El Calvario	2600 ± 40	2740 ± 30	2770	2710	Houbart, 2014
EMOSITE5ECH2	Base El Calvario	9570 ± 60	10955 ± 215	11170	10740	Houbart, 2014
VE3-210106-1	8.5 m SWS	6850 ± 60	7752 ± 57	7820 7800	7810 7580	Riquelme et al., 2011
VE3-210106-2	0.8 m NES	9820 ± 70	11410 ± 85	11590 11400	11560 11090	Riquelme et al., 2011
QC_N24_3	Alluvial deposits	9429 ± 34	8713 ± 93	8806	8621	Calderon, 2021
QC_N24_16	Alluvial deposits	9452 ± 55	8733 ± 126	8860	8607	Calderon, 2021
QC_N24_27	Alluvial deposits	9282 ± 43	8486 ± 145	8631	8341	Calderon, 2021
Fec_40C1	El Calvario	9663 ± 35	10948	10775	11178	Honores, 2021
Fec_107C1	El Calvario	9315 ± 54	10453	10257	10645	Honores, 2021
Fec_145C1	El Calvario	9650 ± 45	10945	10764	11174	Honores, 2021
Fec_150c1	El Calvario	9456 ± 25	10645	10524	10748	Honores, 2021
FEC_M158	El Calvario	6577 ± 33	7457	7370	7558	Honores, 2021
FEC-BS1	El Calvario	7663 ± 29	8409	8376	8510	Honores, 2021

FEC-BS2	El Calvario	5547 ± 37	6303	6223	6392	Honores, 2021
FEC-BS3	El Calvario	4733 ± 35	5385	5321	5565	Honores, 2021
FEC-BS4	El Calvario	2661 ± 23	2750	2726	2768	Honores, 2021
Fec_T3C1	El Calvario	2530 ± 28	2581	2371	2726	Honores, 2021

4. DISCUSSION

3.4 Sedimentary processes

Architectural elements and facies association were used as indicator to interpret hydrodynamic conditions, sedimentary processes, and evolution of the system, additionally geochemical footprint in sediment allow us to interpret the source of the sediment discharge.

3.4.1 Facies association and depositional system

The Architectural Elements (AE) were defined using the Miall (1985) classification attending by their external shape, stratification surface, internal structures organization, and their facies assemblage. The facies association (FA) were defined based on architectural elements and their sedimentary facies. AE allow us to identify geomorphology feature in an ancient system, and their vertical and lateral distribution, to reconstruct the subenvironmental evolution, while FA permit interpret the depositional system behavior as a response to sedimentary process.

alluvial fan (FA3), Braided channel (FA4) and Lacustrine (FA5) (Table 4.1).

Table 4.1. Table that includes the facies association, architectural elements and their interpretation.

Depositional System (DS)	Facies Association (FA)	Architectural Element (AE)	Facies
DS1: Alluvial plain	FA1: Sheet flow and overbank process	FF, SB	Sr, Fl, Fr, C
DS2: Alluvial tributary channel	FA2: Gravel bars and channel	CH, LA	Gt, Gp, St, Fl
DS3: Proximal to medium alluvial fan	FA3: Debris flow	SG	Gmm, Gmg
DS4: Braided channel	FA4: Gravels and sands bars	GB, LA	Gmg, Sp
DS5: Lacustrine	FA5: Stagnant water decantation	-	Fr, C

In the sedimentary succession of the Turbio Valley following AE were recognized: Channels (CH), Gravel Bars and Bedform (GB), Sediment Gravity-flow (SG), Lateral Accretion (LA), Sandy Bedforms (SB); and Floodplain Fines (FF) (Table 4.2). Those reflect different styles of internal bed geometry, and facies assemblage. The Facies Association

trend to the following Depositional Systems (DS): Alluvial plain (FA1), Alluvial tributary channel (FA2), Proximal to medium

3.4.1.1 DS1: Alluvial Plain – Sheet flow and marginal process facies association (FA1)

The facies association 1 (FA1) comprise mudstones with and without organic matter (Fr, C, respectively), siltstones (Fl) and fine-grained sandstones (Sr) (Figure 3.2.A-E, Table **3.1**). Mudstone and siltstones are the most abundant facies and their architectural element correspond to floodplain fines (FF). Some are thin bedded, laminated with climbing ripples (Sr-Fl) or massive with organic matter as detritus (Fc-C) or presents a homogeneous grain-size (Fl-Fr).

Sr facies beds are commonly upward interbedded with mudstone or siltstone (*Fr-Fl*), parallel lamination and particularly climbing ripple cross-lamination in sands are common. Climbing ripples and cross laminations indicate the migration ripples during a high density current in a unidirectional and moderated regime flow, as indicate the asymmetrical ripple features. Sharp-based-2nd order in sandstone beds (Sr) indicate change in hydrodynamic condition through time, related to short-term unsteady flow (Miall, 1988). They are usually thin, less than 20-cm thick and likely to be resulting from *catastrophic overbank on floodplains* from sheet flood on the more distal parts of alluvial fans (Steel & Aasheim, 1978). Sheet-like bed occur in successions lacking major channel and are most likely products of sheet floods on alluvial plains, flow may either emanate from channels or result from local heavy rainfall on the plain itself. The intercalated mudstone with organic matter (Fr-C) is deposited by decantation of the suspension sediment when flow loses velocity, over these deposits an incipient soil is form.

3.4.1.2 DS2: Tributary Channel – Gravel bars and channel facies association (FA2)

Gravel bars and channel facies association is composed by channel (CH) elements infill with lateral accretion (LA) element. They include gravels (Gt, Gp), sandstones (St), and siltstones (Fl) facies. Channel with accretional elements (LA, DA) occur as stacked internal multistorey channel inside a major isolate channel in background of overbank facies (FA1) (Figure **4.1**). 5th-order-bounding surface of Channel element significance an important erosional process and the shifting of the channel position, and multistorey internal channel reflection the lateral mobility of high-energy bedload streams. As is mentioned in section 3.1.1.1 (SWS), the matrix of Gt facies is poorly sorted with more than 30% of mud fraction, and thin siltstones beds to the top of forests is observed. That reflect abrupt diminution of flow and discharge fluctuations in a channel that transport a high suspended sediment (Steel & Thompson, 1983).

3.4.1.3 DS3: Proximal to medium alluvial fan - Debris flow facies association (FA3)

Debris flows facies association include Gmm and Gmg facies and their architectural elements corresponding to Gravity Flow Sediment (GS) (Figure **4.1**).

About sedimentology, matrix-supported conglomerates (Gmm and Gcm) commonly lack of internal bedding and clast imbrication, with some weakly inverse grading and normal grading it may observe. The muddy matrix favors the buoyancy-clasts that promote the cohesiveness of the matrix, this facilitates the transport when interstitial water increases. Also, fabric suggest the forces acting over particles during the transport them, from dispersive pressures caused by particle impacts (inverse gradation) to floatability condition caused likely by local intense turbulence vortices that downstream declining (normal gradation). The fact that it may observe both gradation and massive conglomerates on beds-deposits suggest that during transport the materials have passed through several stages condition (Shultz, 1984) from turbulent to massive flow behavior. That corresponds to density flow, generally regarded as the products of cohesive debris flow (Nemec & Steel, 1984).

3.4.1.4 DS4: Braided Channel system –Gravels and sands bars facies association (FA4)
Braided channel bars facies association comprise gravels bars and bedform (GB), and lateral accretion (LA) elements. GB include matrix-supported, well-sorted imbricated gravels with well-sorted sands matrix facies (Gmg), and LA include cross-bedded coarse sandstone with abundant ryzolithe bioturbation facies (Sp).

GB elements comprise sheet of flat-bedded with bounding surface of 3rd-order between them. Bounding surface significance medium-term change in hydrodynamic condition related to stage fluctuation of flow across a bar form. Flat-bedded of gravels bedforms elements (Gmg) is formed by vertical accretion on longitudinal bars and suggest deposition at high water stages (e.g., Rust, 1984).

LA element comprises wedge- or sheet-like bedform, with internal planar cross stratification of coarse sandstones (Sp), that is interpreted as migration of lateral and transverse bedform in a medium hydrodynamic regimen. Sometimes the topmost layer shows disturbed bedding due to plant growth and organisms during subaerial stage. The lateral and vertical association from LA and GB may be interpreted as conglomeratic braided fluvial configuration.

3.4.1.5 DS5: Lacustrine system – biogeochemical processes facies Association (FA5)
The lacustrine facies association are characterized by rhythmites, a sequence of finely laminated, regular alternations of two or more contrasting sediment facies, as mud-silt with Ox Fe (Fr-Ox Fe), Mud-silt with Ox Mn (Fr-Ox Mn) and mud-silt ripples with coal laminated (Fr-C). Sediment are a combination of clastic (muds-silts), authigenic minerals (gypsum, hematite, and pyrolusite) and organic matter (coal, and wood debris). Individual rhythms can be shown to represent a single year’s sediment accumulation. Wavy ripples likely is the results of movement water by wind, are the most common structure in shallower lake. A Fe-rich temperate lakes examples (Allen., 1996) demonstrates the rhythmicity of the sediment during the winter and summer period. Those layers deposited during the winter comprise organic-rich mud settles from suspension, while those deposits

during spring comprise sediment whit iron precipitation (Ox Fe and Mn), and during summer sediment with diatom accumulation or siliciclastic sediment authigenic minerals (Allen., 1996). This rhythmicity is observable in the lacustrine deposits defined in this work (Figure **3.3**).

Table 4.2. Architectural elements defined to the present work and their principal characteristics.

Architectural element (Miall, 1996)	Bounding surfaces	Facies assemblage	Geometry	Photography
Channel (CH)	5th-order	St, Gt	Concave base, asymmetrical and accretion fill.	
Gravel Bars and Bedform (GB)	3rd-order	Gp	Lens and tabular bodies	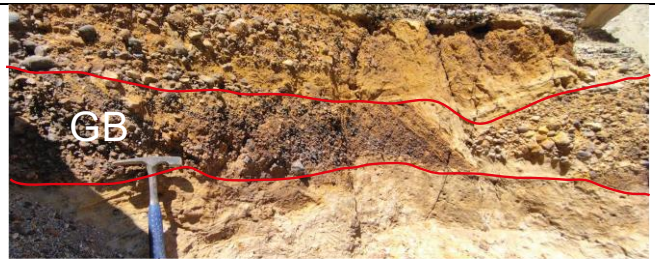
Sediment Gravity Flow (SG)	4th-order	Gmg, Gmm, Gcm	Sheet bedform	

Architectural element (Miall, 1996)	Bounding surfaces	Facies assemblage	Geometry	Photography
Lateral Accretion (LA)	3rd-order	St, Sp, Gt	Wedge, lobe; characterized by internal lateral-accretion.	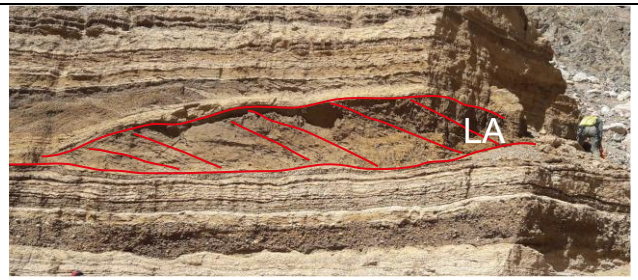
Sandy Bedform (SB)	2nd-order	St, Sp, Sr	Sheet, wedge	
Flood plain fine (FF)	2nd-order	C, Fl, Fr	Sheet	

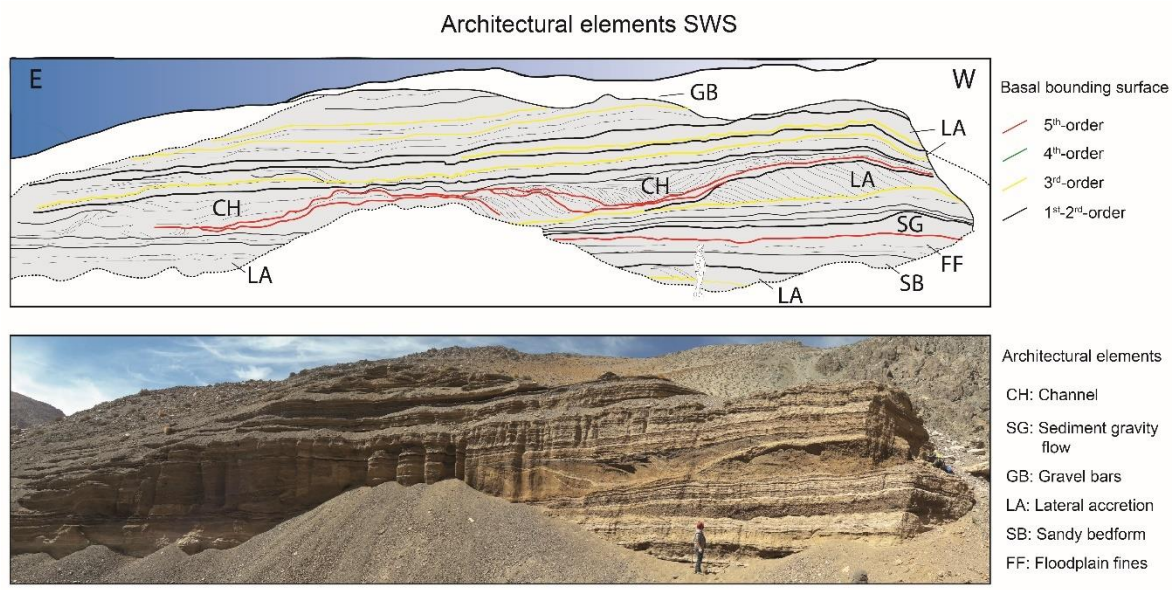

Figure 4.1. Architectural elements from SWS

3.4.2 Source of the sediment

The chemical composition of sediments is extremely diverse, reflecting the variability of the mineralogical composition of them. Terrigenous sediments are products of physical and chemical weathering and erosion of upper crustal rocks exposed at Earth's surface. Thus, chemical, and mineralogical data are useful to obtain information on the primary character of original rocks. That permits us to interpret the source of the sediments and with that the distance of the sediments transport, that may be associated with the runoff intensity and the sedimentary processes.

The Turbio drainage basin is over homogeneous calc-alkaline intrusive, volcaniclastics, and sedimentary rocks. The easter surface of the high Elqui basin the Toro, Seco and La Laguna to Turbio River throughout over pyroclastic and volcanoclastic rocks surface (Salazar and Coloma, 2016). The head of the Toro, Seco and El Tapado River present hydrothermal alteration, and Au-Ag-Cu mineralization zones. The high concentration elements as S, Cu, Mo, As, Sb, Hg and Ti in sediments transport by the river are associated to El Indio-Tambo district, while the low concentration are associated to rock without the hydrothermal alteration and mineralization, as Elqui-Limari Batholith (BEL) and Mesozoic volcanosedimentary rocks (Miralles., 2013). On the other hand, sediment composition may be influenced by physical selection of the particle transport in the water, resulting in an enrichment of heavy minerals and elements such as Fe, Ti, Zn, Mg, in the coarser sediments.

Thus, the main sediment sources that may be controlling the geochemistry of the fluvial sediments in the Turbio River are characterized as: (1) Rocks with hydrothermal

alteration and/or mineralization; and (2) Cretaceous Volcano-Sedimentary Rocks and Paleozoic Intrusive Rocks, without mineralization (Oyarzún et al., 2003; Miralles, 2013).

(1) The Toro and Seco rivers erode large areas with hydrothermal alteration of Neogene age. They are located in the most important mining districts of the Elqui basin: El Indio-Tambo and Carmen de Río Seco (Figure 6.2). Studies of fluvial sediments from the Elqui River indicate that sediments from this area have high concentrations of As, Cu, total S, Ti, Bi, Ni, Se, Sr, and Zn.

(2) The volcano-sedimentary rocks of Cretaceous age show high concentrations of Al2O3, CaO, Fe2O3 and MgO, compounds that can be associated with aluminosilicates, ferromagnesian minerals, and calcite. Meanwhile, the Paleozoic intrusive rocks without mineralization, of the Elqui-Limari batholith. They show high concentrations of Cd, K2O, SiO2, Be, HREE, LREE, Rb, Sn.

There is a relationship between the granulometry and the Cps of the elements, Si, Al, and K, are found mostly in the muddy sediments. On the contrary, these elements decrease in sandy sediments and the Cps of Fe and S increase.

In the NWS, geochemical variations are observed between the muddy sediments of the base and the roof. At the base, over the alluvial gravel facies, strata of mud and silt are superimposed, with local levels of fine sand (Figure 5.8). In the muddy facies, interpreted as flood plains, high values of Si, Al, and K, and low Fe and S, characteristic of finer sediments, were found. Two peaks with increased levels of Zn, Mn and Cu are present (2 and 3m Figure 5.8). This suggests an increase in sediments from rocks with Cu mineralization, accompanied by Zn and Mn (Figure 6.2). Unlike the upper muddy facies (above 4m), interpreted as lacustrine facies, the main elements of the clays (Si, Al, and K) are observed, but also show low Cps of Cu, Zn, Ti, Mn and S unlike the lower muddy facies. This suggests a concentration of elements associated with the alteration of rocks without mineralization, such as intrusives. The fine sand facies, which are interpreted as flood flows, present low Cps of Si, Al and K and high Cps of Fe and S. Like the muddy sediments, the sands differ geochemically between the lower (~4m) and upper (~10m) sand level, the lower one presenting high level of Ca, S, Ti, Mn and Sr, while the upper one does not present Ca, Ti, and Sr, but does contain Cu and Zn. Therefore, it is interpreted that the lower sands present elements associated with volcano-sedimentary rocks (Fe and Ca) without Cu mineralization.

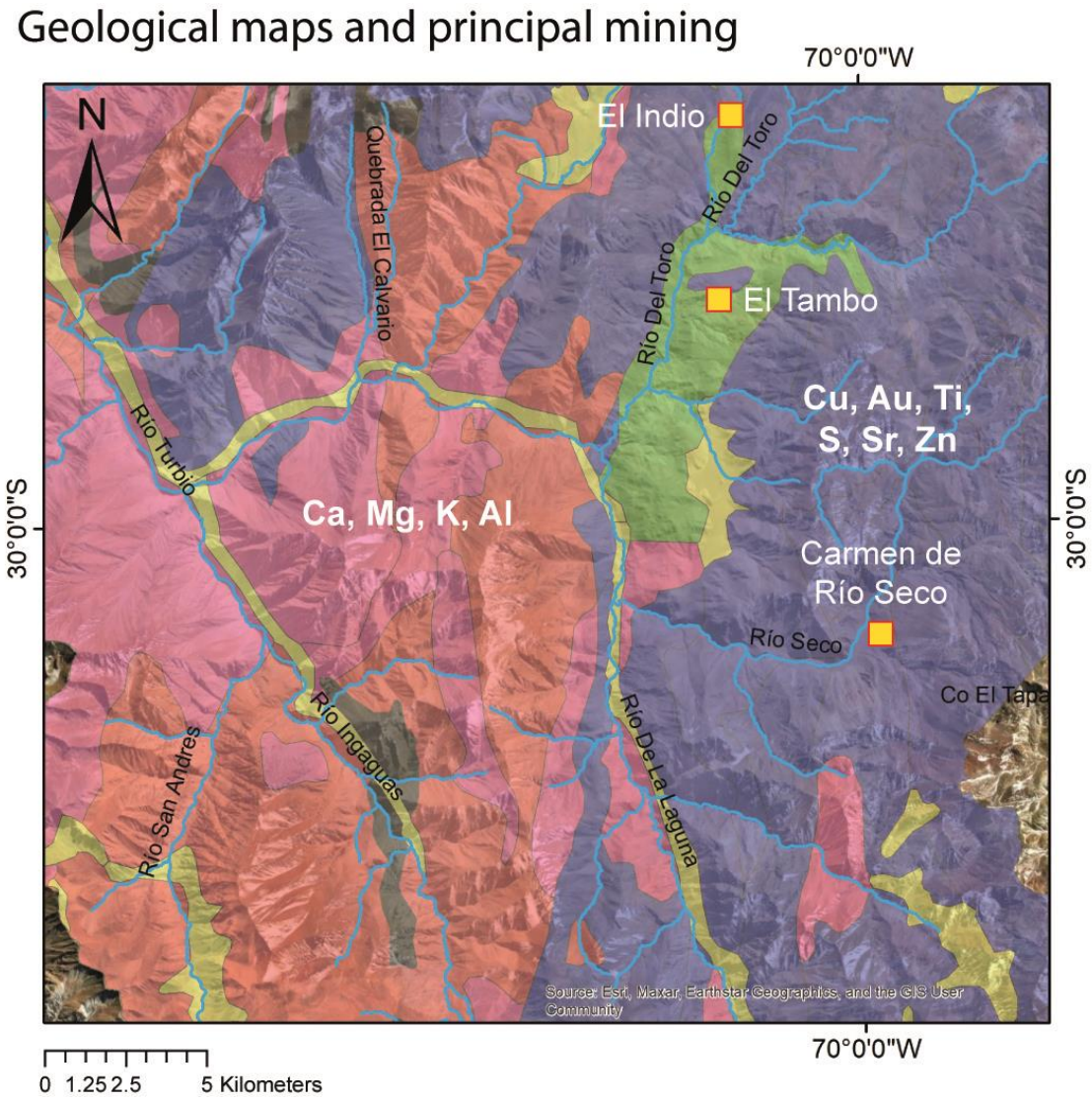

Figure 4.2. Geological map with main zones of economic mineralization (El Tambo and Carmen de Río Seco) and the main features associated with possible sediment sources.

In NES there is a great viability of facies in the succession, being more abundant the facies with sandy matrix at the base and muddy sediments at the top, and they present those main elements associated to their granulometry, as in the previous deposit. The sandy sediments are the only ones that show geochemical differences, they present high concentrations of Zn, Mn, Cu and Sr, with an increasing trend. This implies that the origin of rocks with Cu mineralization increases, while towards the base it decreases, while elements such as Si, Al, and K increase at the same time, elements more characteristic of Paleozoic intrusive rocks.

3.5 Paleoenvironment and climate reconstruction

3.5.1 Paleo-hydrological Evolution

Paleo-hydrological reconstruction scheme from Turbio river valley, were developed to visualize the fluvial dynamic and evolution of their subenvironment during the Early Holocene (Figure 4.5). It was possible to identify the interaction to the principal fluvial channel, with floodplain, alluvial fans, and shallower ephemeral lakes, using the results obtained in this research and others from the Turbio valley (Riquelme et al., 2011; Honores, 2021; Calderon, 2021).

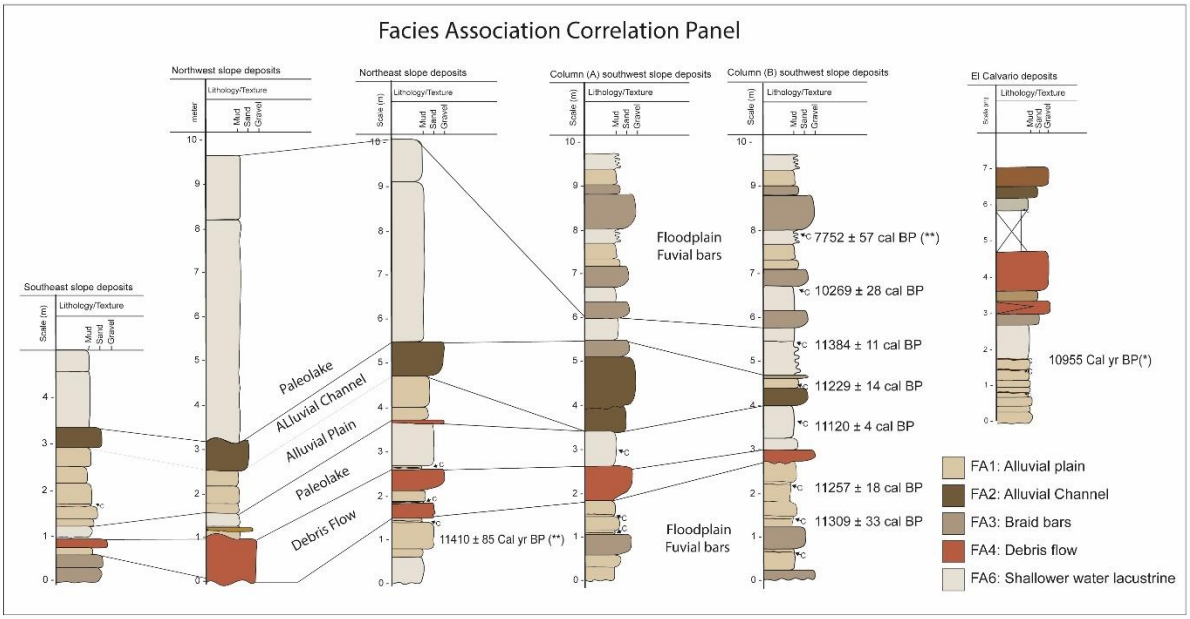

Figure 4.3. Facies association correlation panel.

Respect to our results, a correlation panel (Figure **4.3**) were elaborated using the age, lithology, and geochemistry as a criterion of correlation, to the paleoenvironment reconstruction (**Figure 4.5**). The oldest sediments (11410 ± 85Cal yr Bp; Riquelme et al., 2011) are located at the base of the deposits (Figure 4.3; SWS-Column B) and correspond to the floodplain environment, with the development of sheet flow, and flooding process due the overbank channel from the river. This are superposed by bedding conglomerates associated to the distal part of alluvial fan from Los Piuquenes creek (Figure 1.3; Figure 4.3, AF1) after the 11309 ± 33 cal BP. That event generates the detachment of the river forming a shallowed small lake in 11120 ± 4 cal BP. Subsequently to lacustrine facies, a major alluvial event from Los Piuquenes creek, was described as a debris flow and channel tributary process. That event provokes the damming of the fluvial channel, forming a large lacustrine system, where the depth lake increases towards the eastern deposits (Figure 4.3, NES, SES). The rest of the succession was interpreted as

floodplain environment with overbank and accretion bars process of the fluvial channel, that is correlated with the interpretation of Riquelme et al. (2011) and suggest an age of 7752 ± 57 cal BP to the sediments.

In the El Calvario ravine, a perpendicular tributary to the Turbio River valley, important sedimentary deposits have been recognized on the northern and southern slopes of ravine. An important alluvial fan deposit has been recorded in the northern part of the ravine, this fan has a north-south orientation and has been characterized as a alluvial fan with debris flow processes, characterized as intercalations between deposits of massive gravels and laminated coarse sands. To the south of the ravine a succession of fine, sandy and gravelly sediments is exposed, which have been studied in this and other works. Honores (2021) obtained ages from 10948 cal BP to 2581 cal BP and interpreted depositional processes such as: debris flows, flood inundation, flood plains, and lake formation associated with the damming of the main river. These paleoenvironments have varied during the Holocene, as shown in Figure 6.4. Twenty-eight km downstream is the town of Huanta, where the alluvial fan of the Estero de Huanta stream is located. This fan has been studied by Calderón (2021), his sedimentological and chronostratigraphic analyses indicate the development of debris flows between 8800 and 8300 years BP, immediately above the floodplain deposits (Figure 6.4). The sedimentary processes and paleoenvironments interpreted in the work of Honores and Calderón have also been interpreted in the deposits of the Los Piuquenes-El Calvario segment (Figure 6.3). In this way, a comparison table of the different depositional events and their ages has been made in order to understand the fluvial evolution of the Turbio River during the Holocene.

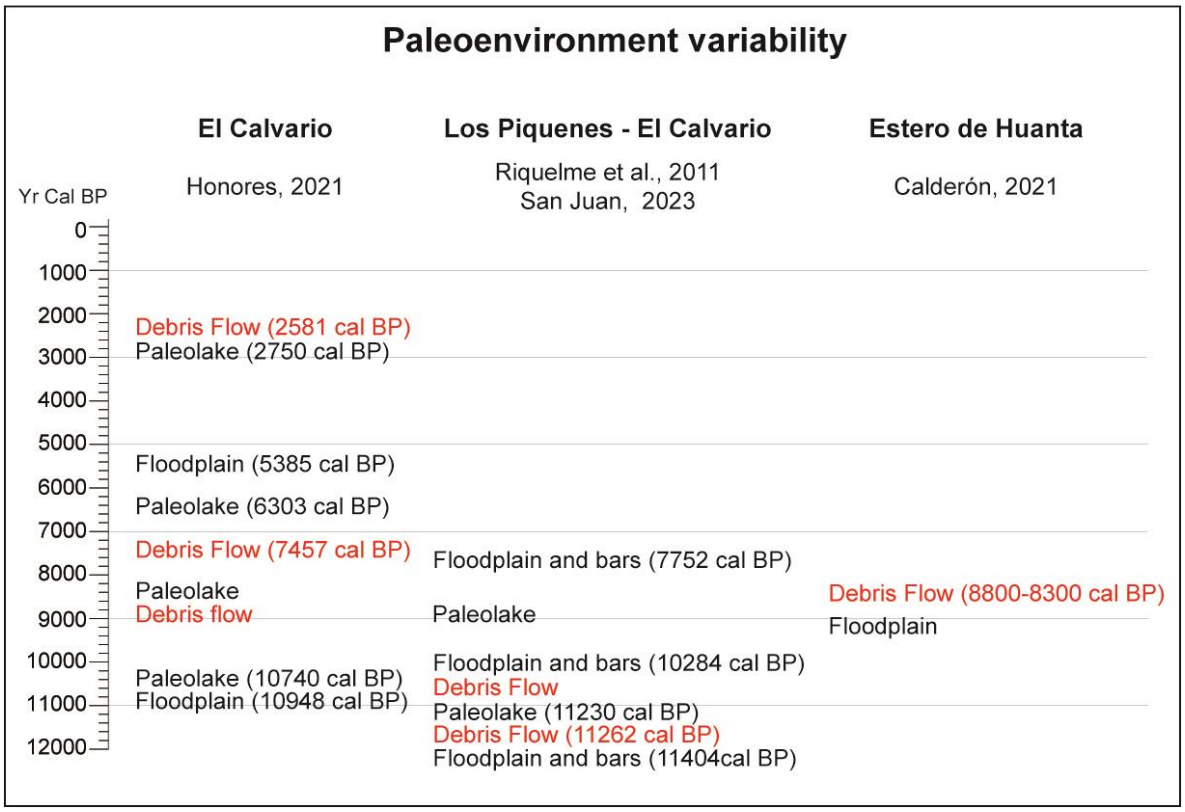

Figure 4.4. Sedimentary process variability in the sediments from the tributaries of Turbio River, El Calvario, Los Piuquenes and Estero de Huanta.

In this way, the evolution of the sedimentary dynamics of the Turbio River is interpreted (Figure 4.5). During the early Holocene (11404 - 10284 cal BP), the formation of a valley with stable fluvial flood plains is interpreted, with the subsequent formation of two large alluvial fans fed by the estuaries coming from Los Piuquenes Creek and another one in El Calvario Creek. This event caused the modification of the fluvial dynamics during this period, causing the stagnation of the main river, giving rise to ephemeral lakes located near to the fans. Subsequently, alluvial events become more recurrent, between 10284-7457 cal BP, with the presence of abundant debris flows distinguished in the succession and intercalated with sediment lake of greater extension and depth. Between 7457 - 2581 cal BP, the establishment of extensive floodplains is interpreted, with abundant sheet flows and local debris flows, intercalated with powerful successions of lacustrine origin. This interaction between floodplain and lacustrine system is possibly due to events that increased the fluvial regime, which fed the ephemeral lakes conditioned by the geomorphology left by the large alluvial events.

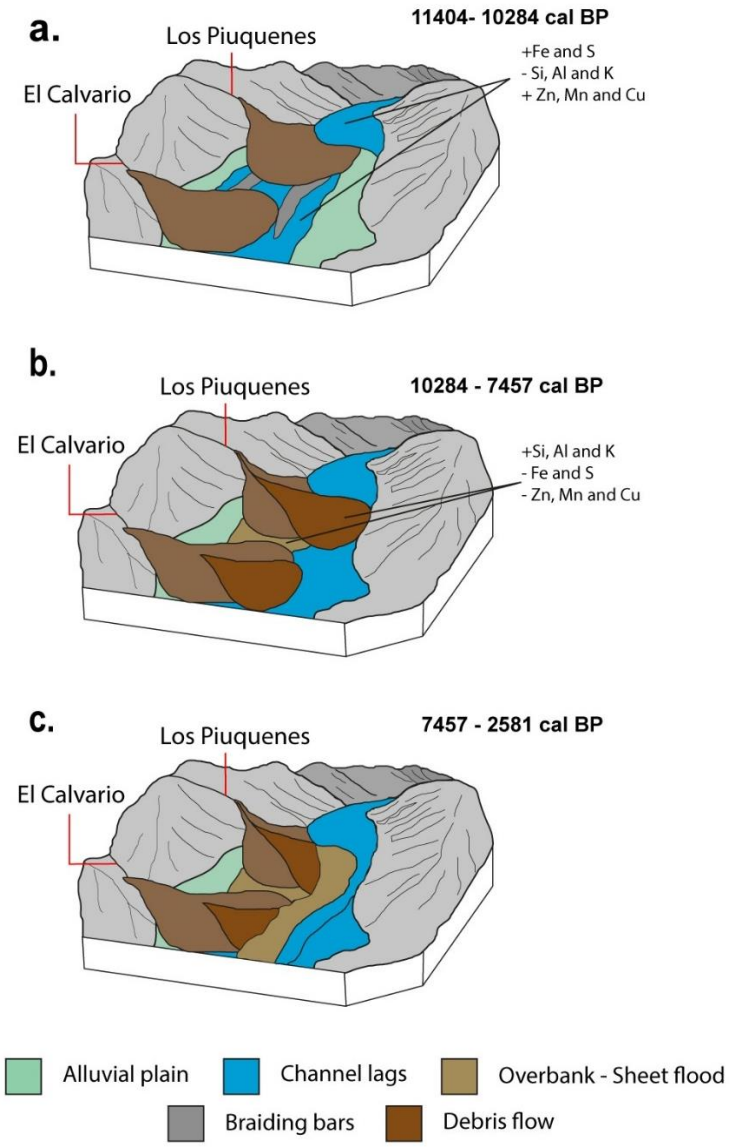

Figure 4.5. Paleoenvironmental evolution in the Río Turbio Valley during the Holocene from Los Piuquenes to El Calvario, and their principal geochemical of the sediment's composition associated to the source of the flow.

3.5.2 Regional Holocene Climatic Implication

Climatic implication of the dynamics in the sedimentary process at the subenvironment is mentioned in term of relative dry environment (major temperature and less-water supply) or humid environment (minor temperature and high-water supply). The most predominant paleo-landscape feature in the valley correspond to floodplain, ephemeral lakes, fluvial bars, and alluvial processes, as sheet flow, debris flow and tributary channel.

About the floodplain, the developmental of paleosol levels indicate a longtime exposed of the surface due the steady of the river channel during their low energy

regimen. Sheet flow and river flood processes are considered as local events by the increases of stream flow, the geochemistry also indicate the sedimentary provenance from alteration and mineralization rocks at the upstream of Turbio river. Those characteristics, the steady river, paleosol and local flooding event, permit us interpret as a relatively dry climatic environment (Figure 4.3).

The shallower lakes were formed by alluvial fan detachment the stream water, in fact the lakes facies are usually distinguished after debris flow deposits, but also over alluvial plain deposits. That vertical relationship indicates the generation of a lake over any surface of the valley and likely is attending to the proximity of the alluvial fan and the lake cover extension. Geochemistry signatures indicate a provenance from upstream rocks with mineralization, probably by the input of the fluvial water, confirming the hypothesis of the detachment river. This environment is considered as wet condition, due the excess of water probably fed by the rivers and alluvial water (Figure 4.3).

Alluvial processes, sheet flow, debris flow and tributary channels, are formed during extreme hydrological events, probably associated with heavy precipitation or the combination with melting snow after the accumulation of snow winter. Their geochemistry feature indicates sediments provenance from rock without alteration or mineralization, like the most proximal rocks in the valley. Therefore, these association is linked with a relatively wet climatic period (Figure 4.3).

Braided fluvial system related to the generation of longitudinal and lateral bars gives the signal to the major transport during a high energy regimen flow. The large planar deposits of gravels indicate extensive plains with abundant traction loading, and the lateral variation with large lateral sandbars indicate the channel migration. The change in the principal drainage channels responds to increases fluvial regimen, likely by meltwater from glacier or snow accumulation winter. Therefore, the climate is interpreted as wet period (Figure 4.3).

Considering the above, and the radiocarbon ages obtained in the sedimentary deposits of the Turbio River in Los Piquenes, is possible to interpret a wet period during the early Holocene (11309 ± 33 to 7752 ± 57 yr cal BP) such is interpreted in another research (Riquelme et al., 2011). Including the age, and the sedimentology interpretations of El Calvario and Estero Huanta succession, permit us to reconstruct the paleoclimatic condition during Holocene in the Turbio Valley, and correlation with the Holocene paleoclimatic reconstructions for the semiarid Andes (27° and 33°S) proposed by Cabré et al. (2017), Riquelme et al., (2011), and Tiner et al. (2018) (Figure 6.6), as mentioned below (Figure 4.6).

The sedimentology of the sedimentary deposits at the Los Piquenes, El Calvario and Estero de Huanta, present a succession of alluvial fans and lake formation by damming interpreted as wet periods, between 11,404 and 745 cal yr BP. Paleoclimatic reconstructions research indicate that the Holocene begins as a wet period between 10800 to 9500 cal yr BP, highlighted by debris flow activation and lake level rise in Laguna Cerritos Blancos and Laguna El Cepo (Tiner et al., 2018). However, Cabre et al., (2017) extends this period to ~7500 cal yr BP (Figure 4.6), that is consistent with our interpretation. This could be due to the result of the decreased influence of SEPSA along the subtropical coast of Chile, favoring the occurrence of sporadic convective precipitation events (Ortega et al., 2012).

Subsequently, in the Piuquenes and Calvario stratigraphy, alluvial activity came to a halt, characterized by the development of floodplains and soil formations, and is interpreted as drier condition, likely around ~6303 ± 84 yr Cal BP. The paleoclimatic record indicate that drier conditions remained between ~7500 to 5,500 cal yr BP, being consistent with our interpretation (Cabre et al., 2017; Tiner et al., 2018).

During ~5385 ± 122 yr Cal BP were interpreted an increase of the lacustrine successions, ending with floodplain deposits and fluvial gravelly sediments at 2548 ± 177 yr cal BP (Honores et al., 2021). According to other authors, between 5,500-4,100 yr cal BP, storm activity and recharge were greater, ending at 2200 yr cal BP, initiating a drier period (Riquelme et al., 2011; Cabre et al., 2017; Tiner et al., 2018).

Finally, and from 2200 years BP onwards, the humid period increased the contribution of the source area, producing the erosion and incision of the paleo-lacustrine deposit, allowing the denudation and exposure of the lacustrine stratigraphic outcrops. In conclusion, it has been determined that there is a strong relationship between surface sedimentary processes and past climatic conditions for the semi-arid Andes of central-northern Chile,

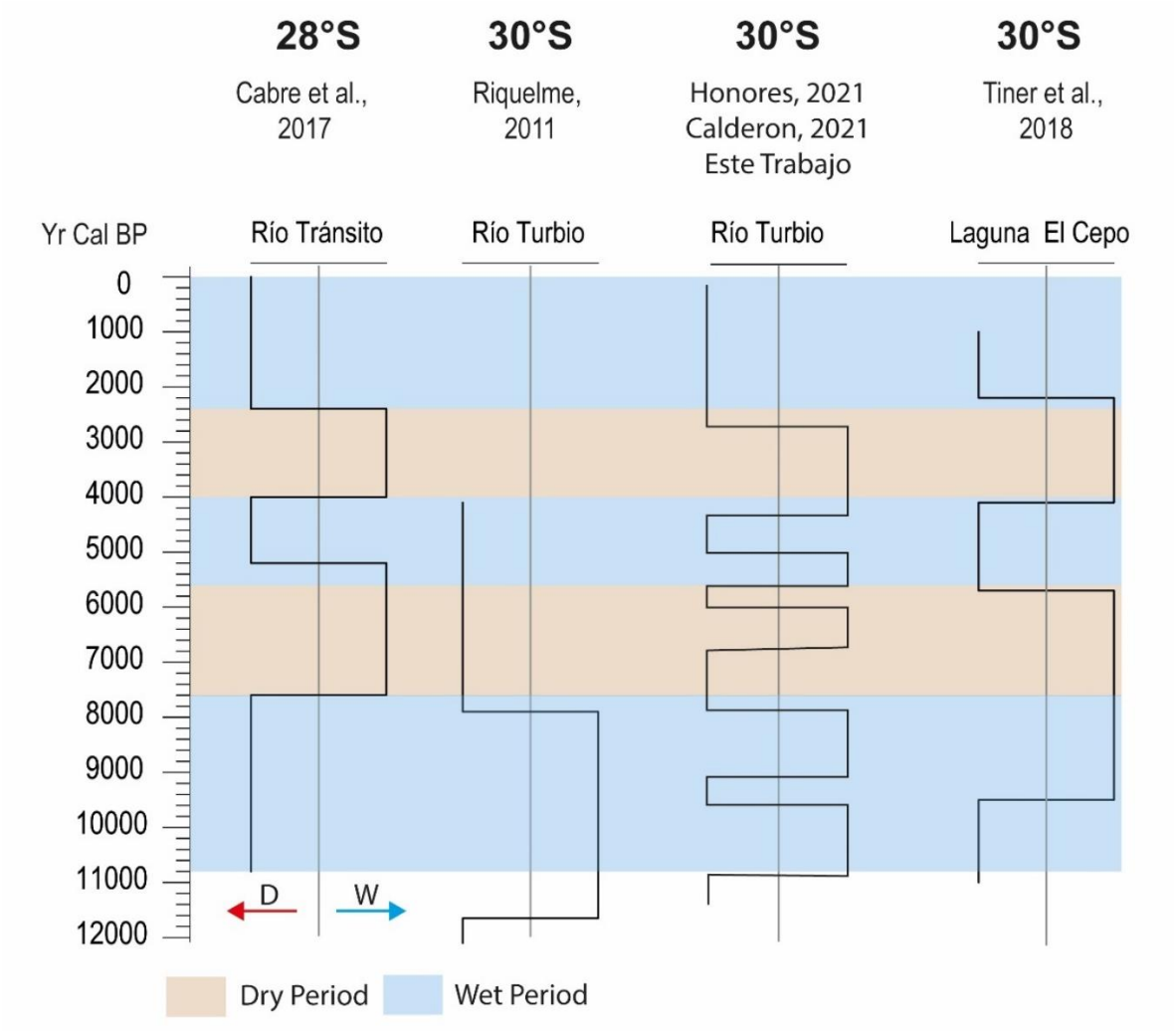

Figure 4.6. Paleoclimatic variability during Holocene in the semiarid region according to other authors and this research.

4 CONCLUSIONS

A Holocene paleoambiental reconstruction has been interpreted in the Turbio Valley, an Andean semiarid valley from north-central Chile, and was using the sedimentology and stratigraphy as a paleoclimatic proxies which is correlated with the paleoclimatic record for the region.

The results indicate that the sedimentary process, as sheet flow, debris flow, lake and alluvial channels suggesting increases stream flow possible associate to wetter climate. In contrast, the establishment of alluvial plain and the generation of a soil, are associated with low energy condition and a steady river channel. Likely associated with decrease of precipitation and dry climate condition. The ages of the sedimentary succession (from 11404 ± 48 to 2548 ± 177 yr cal BP) determine the

chronology of the paleoenvironment reconstruction and were compare with climatic regional data during the Holocene, thi allowed us to state the following.

The Holocene begins as a wet period between 10800 to 7500 cal yr BP, highlighted by debris flow activation, and were associated with the lake level rise in El Cepo lake. The sedimentology of the sedimentary deposits of Los Piuquenes, El Calvario and Estero de Huanta, shows a succession of alluvial fans and lake formation by damming interpreted as wet periods, between 11,404 and 7457 cal yr BP. Subsequently, in the Piuquenes and Calvario stratigraphy is observed an alluvial activity cease by the development of floodplains and soil formations. Then, between 5,500-4,100 cal yr B. P, storm activity and recharge of lake (El Cepo lake) were greater, ending at 2200 cal yr BP, initiating a drier period. This is reflected in the stratigraphy of the paleo-lacustrine deposits of EL Calvario, where the increase in the power of the lacustrine successions is observed, ending with floodplain deposits and fluvial gravelly sediments at 2581 cal yr BP.

Finally, a correlation between the regional palaeoclimate and the sedimentary dynamics of the palaeoenvironments has been determined, concluding the strong relationship between sedimentary surface processes and past climatic conditions for the semi-arid Andes of north-central Chile.

4. CONCLUSIONES

En presente trabajo se realizó la evolución de la dinámica sedimentaria, para reconstruir las variaciones paleoambientes durante Holoceno en el valle del Turbio, un valle semiárido de los Andes del centro-norte de Chile, utilizando la sedimentología y la estratigrafía como indicadores paleoclimáticos los cuales se han correlacionan con los registros paleoclimático de la región.

Los resultados indican que los procesos sedimentarios identificados, como los flujos en lámina, flujos de detritos, lagos y canales aluviales, sugieren posibles aumentos del caudal de los arroyos asociados a un clima más húmedo. Por el contrario, el establecimiento de una llanura aluvial y la generación de un suelo, se asocian con una condición de baja energía y un cauce fluvial más estable. Probablemente asociado a la disminución de las precipitaciones en condiciones climáticas más secas. Las edades de la sucesión sedimentaria (de 11404 ± 48 a 2548 ± 177 años cal BP) determinan la cronología de la reconstrucción paleoambiental y fueron comparadas con los datos climáticos regionales durante el Holoceno, lo cual nos permitió afirmar lo siguiente.

El Holoceno se inicia como un periodo húmedo entre 10800 y 7500 cal yr BP, destacado por la activación de flujos de detritos, y se asocian a la subida del nivel del lago El Cepo en el mismo periodo. La sedimentología de los depósitos

sedimentarios de Los Piuquenes, El Calvario y Estero de Huanta muestra una sucesión de abanicos aluviales y formación de lagos por represamiento interpretados como períodos húmedos, entre 11.404 y 7457 cal yr BP. Posteriormente, en la estratigrafía de los Piuquenes y Calvario se observa un cese de la actividad aluvial por el desarrollo de llanuras de inundación y formaciones de suelos. Luego, entre 5.500-4.100 cal yr B. P, la actividad tormentosa y la recarga del lago (lago El Cepo) fueron mayores, finalizando a los 2200 cal yr BP, iniciándose un período más seco. Esto se refleja en la estratigrafía de los depósitos paleolacustres de EL Calvario, donde se observa el aumento de la potencia de las sucesiones lacustres, finalizando con depósitos de llanura de inundación y sedimentos fluviales gravosos a 2581 cal yr BP.

Finalmente, se ha determinado que existe una fuerte relación entre los procesos sedimentarios superficiales y las condiciones climáticas pasadas para los Andes semiáridos del centro-norte de Chile. Por lo cual, es bastante importante reconocer los cambios en los medios sedimentarios y la dinámica de sus procesos en el pasado, para poder conocer el futuro de los ambientes de montaña actuales debido a los fuertes cambios del clima que se han estado observado en todo el planeta.

5 BIBLIOGRAFÍA

Aceituno, P., 1988. On the functioning of the Southern oscillation in the South American sector. Part I. Surface climate. Monthly Weather Review 116, 505–523.

Baiyegunhi C, Liu K, Gwavava O (2017) Grain size statistics and depositional pattern of the Ecca groups and stones, Karoo Supergroup in the eastern Cape Province, South Africa. Open Geosci 9:554–576

Blott S.J., Pye, K., GRADSTAT: A Grain Size Distribution and Statistics Package for The Analysis of Unconsolidated Sediment. Earth Surface Process. Landforms, 2001, 26, 1237-1248 Search in Google Scholar

Boggs SJ (2009) Petrology of sedimentary rocks, 2nd edn. Cambridge University Press, Cambridge

Cabré Cano, A., Aguilar Martorell, G., & Riquelme Salazar, R. (2017). Holocene evolution and geochronology of a semiarid fluvial system in the western slope of the Central Andes: AMS 14 C data in El Tránsito River Valley, Northern Chile. Quaternary International, 438, 20–32.

Cabre, A., Aguilar, G., Riquelme, R., 2017. Holocene evolution and geochronology of a semiarid fluvial system in the western slope of the Central Andes: AMS 14C data in El Transito River Valley, Northern Chile. Quat. Int. 438, 20–32.

Cai, W., Lengaigne, M., Borlace, S., Collins, M., Cowan, T., McPhaden, M.J., Timmermann, A., Power, S., Brown, J., Menkes, C., Ngari, A., Vincent, E.M., Widlansky, M.J., 2012. More extreme swings of the South Pacific convergence zone due to greenhouse warming. Nature 488, 365–369.

Cano, A. C., Martorell, G. A., & Salazar, R. R. (2017). Holocene evolution and geochronology of a semiarid fluvial system in the western slope of the Central Andes: AMS 14C data in El Tránsito River Valley, Northern Chile. Quaternary International, 438, 20-32.

Carre, M., Azzoug, M., Bentaleb, I., Chase, B.M., Fontugne, M., Jackson, D., Ledru, M.-P., Maldonado, A., Sachs, J.P., Schauer, A.J., 2012. Mid-Holocene mean climate in the South-Eastern Pacific and its influence on South America. Quat. Int. 253, 55–66.

Carvalho LM, Jones C, Posadas AN, Quiroz R, Bookhagen B, Liebmann B. 2012. Precipitation characteristics of the South American monsoon system derived from multiple datasets. J. Clim. 25(13): 4600–4620.

Curtis, S., & Adler, R. F. (2003). Evolution of El Niño-precipitation relationships from satellites and gauges. Journal of Geophysical Research: Atmospheres, 108(D4).

Dai, A., Wigley, T.M.L., 2000. Global patterns of ENSO-induced precipitation. Geophys.

Garreaud R, Vuille M, Compagnucci R, Marengo J. 2009. Present-day South American climate. Palaeogeogr. Palaeoclimatol. Palaeoecol. 281(3–4): 180–195, doi: 10.1016/j.palaeo.2007.10.032.

Garreaud, R. D., Boisier, J. P., Rondanelli, R., Montecinos, A., Sepúlveda, H. H., & Veloso-Aguila, D. (2020). The central Chile mega drought (2010–2018): a climate dynamics perspective. International Journal of Climatology, 40(1), 421-439.

Garreaud, R., Aceituno, P., 2002. Atmospheric circulation over South America: mean features and variability. In: Young, K. (Ed.), the Physical Geography of South America. Oxford University Press.

Garreaud, R., Rutllant, J.A., 1996. Analisis meteorologico de los aluviones de Antofagasta y Santiago de Chile en el periodo 1991–1993. Atmosfera 9, 251–271.

Gunten, L., 2016. Late Holocene environmental changes as recorded in the sediment of high Andean Laguna Chepical, Central Chile (32°S;3050 m a.s.l.). Palaeogeogr. Palaeoclimatol. Palaeoecol. 461, 44–54.

Jenny, B., Wilhem, D., Valero-Garces, B.L., 2003. The Southern Westerlies in Central Chile: Holocene precipitation estimates based on a water balance model for Laguna Aculeo (33°50′S). Clim. Dyn. 20 (2), 269–280.

Kaiser, J., Schefub, E., Lamy, F., Mohtadi, M., Hebbeln, D., 2008. Glacial to Holocene changes in sea surface temperature and coastal vegetation in north Central Chile: high versus low latitude forcing. Quat. Sci. Rev. 27, 2064–2075.

Kim, J.-H., Schneider, R.R., Hebbeln, D., Muller, P.J., Wefer, G., 2002. Last deglacial sea surface temperature evolution in the Southeast Pacific compared to climate changes on the south American continent. Quat. Sci. Rev. 21, 2085–2097.

Lauro, C., Moreiras, S. M., Junquera, S., Vergara, I., Toural, R., Wolf, J., & Tutzer, R. (2017). Summer rainstorm associated with a debris flow in the Amarilla gully

affecting the international Agua Negra Pass (30° 20′ S), Argentina. Environmental Earth Sciences, 76(5), 213.

Maldonado, A., & Villagrán, C. (2006). Climate variability over the last 9900 cal yr BP from a swamp forest pollen record along the semiarid coast of Chile. Quaternary Research, 66(2), 246-258.

Maldonado, A., Villagran, C., 2002. Paleoenvironmental changes in the semiarid coast of Chile (~32°S) during the last 6200 cal years inferred from a swampforest pollen record. Quat. Res. 58, 130–138.

Maksaev, V.; Munizaga, F.; Tassinari, C. 2014. Timing of the magmatism of the paleo-Pacific border of Gondwana: U-Pb geochronology of Late Paleozoic to Early Mesozoic igneous rocks of the north Chilean Andes between 20° and 31°S. Andean Geology 41 (3): 447-506. doi: 10.5027/andgeoV41n3-a01

Marengo JA, Liebmann B, Grimm AM, Misra V, Silva Dias PL, Cavalcanti IFA, Carvalho LMV, Berbery EH, Ambrizzi T, Vera CS, Saulo AC, Nogues-Paegle J, Zipser E, Seth A, Alves LM. 2012. Recent developments on the South American monsoon system. Int. J. Climatol. 32(1): 1–21.

Meza Albornoz, C. P. (2019). Aluviones históricos y prehistóricos en la ciudad de Taltal, Región de Antofagasta. Tesis de Pregrado, Departamento de Geología, Universidad de Chile, Santiago.

Miller, A., 1976: The climate of Chile. Climates of Central and South America, W. Schwerdtfeger, Ed., Elsevier, 113–145

Mo, K.C., Higgins, R.M., 1998. The Pacific–South American modes and tropical convection during the Southern Hemisphere winter. Mon. Weather Rev. 126, 1581–1596.

Montecinos, A., & Aceituno, P. (2003). Seasonality of the ENSO-related rainfall variability in central Chile and associated circulation anomalies. Journal of climate, 16(2), 281-296.

Moreiras S, Lisboa MS, Mastrantonio L. The role of snow melting upon landslides in the central Argentinean Andes. Earth Surf Process Landforms. 2012;37(10):1106-1119.

Ortega, C., Vargas, G., Rojas, M., Rutllant, J. A., Muñoz, P., Lange, C. B., ... & Ortlieb, L. (2019). Extreme ENSO-driven torrential rainfalls at the southern edge of the Atacama Desert during the Late Holocene and their projection into the 21th century. Global and planetary change, 175, 226-237.

Ortega, C., Vargas, G., Rutllant, J., 2013. Major hydrological regime change along the semiarid western coast of South America during the early Holocene – response to comments by Maldonado and Moreiras. Quat. Res. 80, 140–142.

Ortega, C., Vargas, G., Rutllant, J.A., Jackson, D., Mendez, C., 2012. Major hydrological regime changes along the semi-arid western coast of South America during the early Holocene. Quat. Res. 78, 513–527.

Ortiz, M.; Merino, R.N. 2015. Geología de las áreas Río Chollay-Matancilla y Cajón del Encierro, regiones de Atacama y Coquimbo. Servicio Nacional de Geología y Minería, Carta Geológica de Chile, Serie Geología Básica 175-176, 1 mapa escala 1:100.000.

Oyarzún, J., Maturana, H., Paulo, A., & Pasieczna, A. (2003). Heavy metals in stream sediments from the Coquimbo Region (Chile): effects of sustained mining and natural processes in a semi-arid Andean basin. *Mine Water and the Environment*, *22*(3), 155-161.

Paskoff R., 1970: Le Chili semi-aride, recherches géomorphologiques.Editions Biscaye Frères, Bordeaux, 420 p.

Power, S., Delage, F., Chung, C., Kociuba, G., Keay, K., 2013. Robust twent-first-century projections of El Nino and related precipitation variability. Nature 502, 541–545. https://doi.org/10.1038/nature12580.

Quintana J, Aceituno P. 2012. Changes in the rainfall regime along the extratropical west coast of South America (Chile): 30 – 43◦S. Atmósfera 25(1): 1–22.

Riquelme, R., Rojas, C., Aguilar, G., & Flores, P. (2011). Late Pleistocene–early Holocene paraglacial and fluvial sediment history in the Turbio valley, semiarid Chilean Andes. Quaternary Research, 75(1), 166-175.

Rutllant, J., Fuenzalida, H., 1991. Synoptic aspects of central rainfall variability associated with the Southern Oscillation. Int. J. Climatol. 11, 63e76.

Rongier, G., & Peeters, L. (2022). How Fluvial Deposits Distort Aquifer Recharge Estimated From Groundwater Age: Insights From a Landscape Evolution Model. Water Resources Research, 58(3), e2021WR030963.

Salazar, E.; Coloma, F. 2016. Geología del área Cerros de Cantaritos-Laguna Chica, Región de Atacama. Servicio Nacional de Geología y Minería, Carta Geológica de Chile, Serie Geología Básica 181: 171 p., 1 mapa 1:100.000.

Saeid, E., Kendall, C., Kellogg, J., De Keyser, T., Hafiz, I., Albesher, Z., & Martinez, J. A. (2022). A depositional model for the Carbonera Formation, Llanos Foothills,

Colombia, from workflow of a sequence stratigraphic framework and interpretation from well-log stacking patterns, well cuttings, and three-dimensional seismic spectral decomposition. AAPG Bulletin, 106(2), 321-353.

SERNAGEOMIN, 2003. Mapa Geológico de Chile: versión digital. *Servicio Nacional de Geología y Minería, Publicación Geológica Digital,* No. 4 (CD-ROM, versión1.0, 2003). Santiago.

Sahu B.K., Depositional mechanism from the size analysis of elastic sediment. Journal of Sedimentary petrology, 1964, 34(1), 73-83 Search in Google Scholar

Schulz, N., Boisier, J.P., Aceituno, P., 2011. Climate change along the arid coast of northern Chile. Int. J. Climatol. 32 (12), 1803–1814. https://doi.org/10.1002/joc.2395.

Stuiver, M., Reimer, P.J., and Reimer, R.W., 2021, CALIB 8.2 [WWW program] at http://calib.org.

Tiner, R. J., Negrini, R. M., Antinao, J. L., McDonald, E., & Maldonado, A. (2018). Geophysical and geochemical constraints on the age and paleoclimate implications of Holocene lacustrine cores from the Andes of central Chile. Journal of Quaternary Science, 33(2), 150-165.

Valdés-Pineda R, Pizarro R,Valdés JB, Carrasco JF, García-Chevesich P, Olivares C. 2015. Spatio-temporal trends of precipitation, its aggressiveness and concentration, along the Pacific coast of South America (36◦ –49◦ S). Hydrol. Sci. J. (in press).

Vargas, G., Rutllant, J., Ortlieb, L., 2006. ENSO tropical–extratropical climate teleconnections and mechanisms for Holocene debris flows along the hyperarid coast of western South America (17°–24°S). Earth Planet. Sci. Lett. 249, 467–483.

Vergara Dal Pont, I., Moreiras, S. M., Santibanez Ossa, F., Araneo, D., & Ferrando, F. (2020). Debris flows triggered from melt of seasonal snow and ice within the active layer in the semi-arid Andes. Permafrost and Periglacial Processes, 31(1), 57-68.

Vicuña, S., Gironás, J., Meza, F. J., Cruzat, M. L., Jelinek, M., Bustos, E., … Bambach, N. (2013). Exploring possible connections between hydrological extreme events and climate change in central south Chile. Hydrological Sciences Journal, 58(8), 1598–1619. https://doi.org/10.1080/02626667.2013.840380

Villagran, C., Varela, J., 1990. Palynological evidence for increased aridity on the central Chilean coast during the Holocene. Quat. Res. 34, 198–207.

Villa-Martínez, R., Villagrán, C., & Jenny, B. (2003). The last 7500 cal yr BP of westerly rainfall in Central Chile inferred from a high-resolution pollen record from Laguna Aculeo (34 S). Quaternary Research, 60(3), 284-293.

Villa-Martinez, R., Villagran, C., Jenny, B., 2003. The last 7500 cal yr BP of westerly rainfall in Central Chile inferred from a high-resolution pollen record from Laguna Aculeo (34°S). Quat. Res. 60, 284–293.

Ward, P.J., Jongman, B., Kummu, M., Dettinger, M.D., Spema Weiland, F.C., Winsemius, H.C., 2014. Strong influence of El Niño Southern Oscillation on flood risk around the world. PNAS 111, 15659–15664.

Zech, R., Kull, C., Veit, H., 2006. Late Quaternary glacial history in the Encierro valley, northern Chile (29°S), deduced from 10Be surface exposure dating. Palaeogeography, Palaeoclimatology, Palaeoecology 243, 277–286.

Zech, R., Kull, R., Kubik, P.W., Veit, H., 2007. Exposure dating of Late Glacial and pre-LGM moraines in the Cordon de Doña Rosa, Northern/Central Chile (31°S). Climate of the Past Discussions 3, 1–14.

Zech, R., May, J.-H., Kull, C., Ilgner, J., Kubik, P.W., Veit, H., 2008. Timing of the late Quaternary glaciations in the Andes from 15 to 40°S. Journal of Quaternary Science 23 (6–7), 635–647.

Zhang, Z., Li, Z., Deng, X., Liao, J., & Zheng, X. (2022). Multi-parameters logging identifying method for sand body architectures of tight sandstones: A case from the Triassic Chang 9 Member, Longdong area, Ordos Basin, NW China. Journal of Petroleum Science and Engineering, 110824.

Zischg A, Curtaz M, Galuppo A, et al. Permafrost and debris-flows. In: Schoeneich P, Dall'Amico M, Deline P, Zischg A, eds. Hazards related to permafrost and to permafrost degradation. Grenoble, France: PermaNET; 2011:29-66.

6 ANEXO:

Tabla que resume las muestras tomadas para cada afloramiento, la localización estratigráfica (profundidad) y los resultados del análisis granulométrico.

Muestras	Depth	Facies	Textural group	Sediments name	Mode	Mean	ø	Sorting	ø	%mud
Column A-SWS										
01_AN	0.2	Fr	Sandy Mud	Very Fine Sandy Very Coarse Silt	Unimodal	Coarse Silt	5.180	Poorly Sorted	1.129	86.9%
02_AN	0.5	Sr	Sandy Mud	Very Fine Sandy Very Coarse Silt	Unimodal	Very Coarse Silt	4.310	Moderately Sorted	0.947	59.2%
03_AN	0.75	Sp	Sand	Poorly Sorted Coarse Sand	Bimodal	Medium Sand	1.446	Poorly Sorted	1.263	4.7%
04_AN	1.15	Sr	Muddy Sand	Very Coarse Silty Very Fine Sand	Unimodal	Very Fine Sand	3.980	Poorly Sorted	1.116	47.6%
05_AN	1.65	Fr	Sandy Mud	Very Fine Sandy Very Coarse Silt	Bimodal	Very Coarse Silt	4.352	Poorly Sorted	1.241	63.4%
06_AN	2.1	Sp	Muddy Sand	Very Coarse Silty Very Fine Sand	Unimodal	Very Fine Sand	3.051	Moderately Sorted	0.821	12.1%
07_AN	2.9	Fl	Sandy Mud	Very Fine Sandy Coarse Silt	Unimodal	Coarse Silt	5.293	Poorly Sorted	1.484	80.0%
08_AN	3.7	Sp	Sand	Moderately Sorted Fine Sand	Unimodal	Fine Sand	2.715	Moderately Sorted	0.722	3.3%
09_AN	4.5	Gc	Sand	Moderately Well Sorted Coarse Sand	Unimodal	Coarse Sand	0.581	Moderately Well Sorted	0.637	0.1%
10_AN	5.9	Ft	Sandy Mud	Very Fine Sandy Very Coarse Silt	Bimodal	Very Coarse Silt	4.474	Poorly Sorted	1.486	64.5%
Column B-SWS										
21_AN	4.25	Sp	Sand	Moderately Sorted Medium Sand	Unimodal	Medium Sand	1.241	Moderately Sorted	0.724	0.4%
22_AN	4.5	Sr	Muddy Sand	Very Coarse Silty Very Fine Sand	Unimodal	Very Fine Sand	3.495	Moderately Sorted	0.839	25.8%
23_AN	4.8	Sp	Sand	Poorly Sorted Medium Sand	Unimodal	Medium Sand	1.808	Poorly Sorted	1.234	6.5%
24_AN	5.85	Sp	Muddy Sand	Very Coarse Silty Very Fine Sand	Unimodal	Very Fine Sand	3.524	Poorly Sorted	1.415	38.2%
25_AN	6.9	Gmg	Muddy Sand	Very Coarse Silty Fine Sand	Unimodal	Fine Sand	2.748	Poorly Sorted	1.298	16.9%
26_AN	7.1	Fl	Muddy Sand	Very Coarse Silty Medium Sand	Trimodal	Very Fine Sand	3.122	Very Poorly Sorted	2.187	31.2%
27_AN	8.9	Fr	Sandy Mud	Very Fine Sandy Very Coarse Silt	Bimodal	Very Coarse Silt	4.483	Poorly Sorted	1.481	69.3%
SES										
P2_N1	0.2	Sp	Sand	Moderately Sorted Fine Sand	Unimodal	Fine Sand	2.471	Moderately Sorted	0.909	6.3%
P2_N2	0.4	Sp	Sand	Moderately Sorted Fine Sand	Unimodal	Fine Sand	2.503	Moderately Sorted	0.944	7.3%
P2_N3	0.7	Fl	Muddy Sand	Very Coarse Silty Very Fine Sand	Unimodal	Very Fine Sand	3.934	Poorly Sorted	1.144	46.5%
P2_N4	0.9	Gcm	Sand	Moderately Sorted Medium Sand	Unimodal	Fine Sand	2.176	Moderately Sorted	0.953	5.7%
P2_N5	1.2	Fr	Sandy Mud	Very Fine Sandy Very Coarse Silt	Bimodal	Very Coarse Silt	4.575	Poorly Sorted	1.323	71.4%
P2_N6	1.3	Fr	Muddy Sand	Very Coarse Silty Fine Sand	Unimodal	Fine Sand	2.909	Poorly Sorted	1.334	20.0%
P2_N7	1.5	Fl	Muddy Sand	Very Coarse Silty Very Fine Sand	Unimodal	Very Fine Sand	3.570	Moderately Sorted	0.892	29.9%
P2_N8	1.75	St	Muddy Sand	Very Coarse Silty Medium Sand	Unimodal	Fine Sand	2.454	Poorly Sorted	1.201	12.2%
P2_N9	2	Fl	Muddy Sand	Very Coarse Silty Fine Sand	Unimodal	Very Fine Sand	3.108	Poorly Sorted	1.164	20.9%
P2_N10	2.2	Fr	Sandy Mud	Very Fine Sandy Very Coarse Silt	Bimodal	Very Coarse Silt	4.760	Poorly Sorted	1.407	75.6%
P2_N11	2.5	Fl	Muddy Sand	Very Coarse Silty Fine Sand	Unimodal	Very Fine Sand	3.024	Poorly Sorted	1.233	20.8%
P2_N12	3.2	Sp	Muddy Sand	Very Coarse Silty Fine Sand	Unimodal	Very Fine Sand	3.144	Moderately Sorted	0.914	17.0%
P2_N11_techo (P2_N13)	3.5	Fl	Muddy Sand	Very Coarse Silty Fine Sand	Unimodal	Very Fine Sand	3.654	Very Poorly Sorted	2.104	38.0%
P2_N12_techo (P2_N14)	4.5	Fl	Muddy Sand	Very Coarse Silty Fine Sand	Unimodal	Very Fine Sand	3.568	Poorly Sorted	1.952	36.2%
El Calvario										
D2P2_N1 _Calv	0.2	Fr	Sandy Mud	Very Fine Sandy Very Coarse Silt	Unimodal	Very Coarse Silt	4.235	Moderately Sorted	0.906	58.8%
D2P2_N2_Calv	0.3	Fr	Sandy Mud	Very Fine Sandy Very Coarse Silt	Unimodal	Coarse Silt	5.177	Poorly Sorted	1.569	75.3%
D2P2_N3_Calv	0.5	Fr	Sandy Mud	Very Fine Sandy Very Coarse Silt	Unimodal	Very Coarse Silt	4.450	Moderately Sorted	0.888	68.7%
D2P2_N4_Calv	0.75	Fr	Sandy Mud	Very Fine Sandy Very Coarse Silt	Unimodal	Very Coarse Silt	4.319	Poorly Sorted	1.883	53.0%
D2P2_N5_Calv	0.9	Fr	Sandy Mud	Very Fine Sandy Very Coarse Silt	Unimodal	Very Coarse Silt	4.624	Poorly Sorted	1.018	72.7%
D2P2_N6_Calv	1	Fl	Sandy Mud	Medium Sandy Coarse Silt	Bimodal	Very Coarse Silt	4.450	Very Poorly Sorted	2.031	64.6%
D2P2_N7_Calv	1.25	Fr - C	Sandy Mud	Very Fine Sandy Coarse Silt	Unimodal	Coarse Silt	5.494	Poorly Sorted	1.566	83.3%
D2P2_N8_Calv	1.45	Fr	Sandy Mud	Very Fine Sandy Very Coarse Silt	Unimodal	Very Coarse Silt	4.639	Moderately Sorted	0.970	74.1%
D2P2_N9_Calv	1.7	Fr - C	Sandy Mud	Very Fine Sandy Very Coarse Silt	Unimodal	Very Coarse Silt	4.787	Poorly Sorted	1.889	59.6%
D2P2_10_Calv	2.3	Fr - C	Sandy Mud	Very Fine Sandy Very Coarse Silt	Unimodal	Very Coarse Silt	4.393	Very Poorly Sorted	2.069	51.8%
D2P2_11_Calv	2.8	Sp	Sand	Moderately Sorted Fine Sand	Unimodal	Fine Sand	2.483	Moderately Sorted	0.930	7.3%
D2P2_12_Calv	3.5	Sp	Muddy Sand	Very Coarse Silty Fine Sand	Unimodal	Very Fine Sand	3.867	Poorly Sorted	1.982	39.1%
D2P2_13_Calv	6	Fr	Sandy Mud	Very Fine Sandy Very Coarse Silt	Unimodal	Coarse Silt	5.044	Poorly Sorted	1.649	72.2%
D2P2_14_Calv	6.4	Sp	Muddy Sand	Very Coarse Silty Very Fine Sand	Unimodal	Very Fine Sand	3.926	Poorly Sorted	1.863	41.4%
D2P2_15_Calv	7	Gm	Sandy Mud	Very Fine Sandy Very Coarse Silt	Unimodal	Very Coarse Silt	4.704	Poorly Sorted	1.697	65.8%
NWS										
001_AN_S	0.25	Fl	Sandy Mud	Very Fine Sandy Coarse Silt	Bimodal	Coarse Silt	5.088	Very Poorly Sorted	2.187	69.0%
002_AN_S	0.5	Fl	Muddy Sand	Very Coarse Silty Very Fine Sand	Unimodal	Very Fine Sand	3.945	Poorly Sorted	1.888	43.6%
003_AM_S	0.75	Fl	Muddy Sand	Very Coarse Silty Very Fine Sand	Bimodal	Very Coarse Silt	4.021	Poorly Sorted	1.525	48.5%
004_AN_S	1	Fr	Sandy Mud	Very Fine Sandy Very Coarse Silt	Unimodal	Coarse Silt	5.017	Poorly Sorted	1.677	79.8%
005_AN_S	1.33	Fl	Muddy Sand	Very Coarse Silty Very Fine Sand	Unimodal	Very Coarse Silt	4.023	Poorly Sorted	1.543	47.7%
006_AN_S	1.66	Sr	Sand	Moderately Sorted Fine Sand	Unimodal	Fine Sand	2.698	Moderately Sorted	0.965	9.6%
007_AN_S	2	Sr	Sand	Moderately Sorted Fine Sand	Unimodal	Fine Sand	2.333	Moderately Sorted	0.767	3.8%
008_AN_S	4	Fr - C	Sandy Mud	Very Fine Sandy Very Coarse Silt	Unimodal	Very Coarse Silt	4.645	Very Poorly Sorted	2.134	60.6%
009_AN_S	5.5	Fr - C	Sandy Mud	Very Fine Sandy Very Coarse Silt	Unimodal	Coarse Silt	5.224	Poorly Sorted	1.580	83.6%
010_AN_S	7.25	Fr - C	Sandy Mud	Very Fine Sandy Coarse Silt	Bimodal	Coarse Silt	5.284	Poorly Sorted	1.970	80.5%
011_AN_S	8	Fr - C	Sandy Mud	Fine Sandy Coarse Silt	Bimodal	Coarse Silt	5.086	Very Poorly Sorted	2.196	75.9%
012_AN_S	8.3	Fr	Sandy Mud	Fine Sandy Coarse Silt	Bimodal	Coarse Silt	5.603	Poorly Sorted	1.927	84.3%
013_AN_S	8.6	Fr - C	Sandy Mud	Very Fine Sandy Coarse Silt	Bimodal	Very Coarse Silt	4.962	Very Poorly Sorted	2.152	75.0%
014_AN_S	8.9	Sr	Muddy Sand	Very Coarse Silty Medium Sand	Unimodal	Fine Sand	2.303	Poorly Sorted	1.765	15.6%
015_AN_S	9.2	Fr	Sandy Mud	Very Fine Sandy Coarse Silt	Unimodal	Very Coarse Silt	4.928	Very Poorly Sorted	2.079	69.8%
016_AN_S	9.5	Fr - C	Sandy Mud	Fine Sandy Coarse Silt	Bimodal	Coarse Silt	5.113	Very Poorly Sorted	2.596	67.7%
017_AN_S	10	Fr - C	Sandy Mud	Very Fine Sandy Coarse Silt	Bimodal	Very Coarse Silt	4.866	Very Poorly Sorted	2.011	71.9%
NES										
018_AN_S	0.25	Fl	Sandy Mud	Very Fine Sandy Very Coarse Silt	Unimodal	Coarse Silt	5.209	Poorly Sorted	1.438	86.3%
019_AN_S	0.75	Fr	Sandy Mud	Fine Sandy Coarse Silt	Bimodal	Coarse Silt	5.070	Very Poorly Sorted	2.205	71.6%
020_AN_S	1	Sr	Sand	Moderately Sorted Fine Sand	Unimodal	Fine Sand	2.570	Moderately Sorted	0.792	5.0%
021_AN_S	1.25	Gmg	Muddy Sand	Very Coarse Silty Medium Sand	Unimodal	Medium Sand	1.795	Poorly Sorted	1.620	12.3%
022_AN_S	1.75	Sr	Muddy Sand	Very Coarse Silty Very Fine Sand	Unimodal	Very Fine Sand	3.633	Poorly Sorted	1.201	34.8%
023_AN_S	2.25	Gcm	Muddy Sand	Very Coarse Silty Medium Sand	Unimodal	Fine Sand	2.335	Poorly Sorted	1.380	13.2%
024_AN_S	3	Sr	Sand	Moderately Sorted Fine Sand	Unimodal	Fine Sand	2.650	Moderately Sorted	0.950	9.1%
025_AN_S	3.8	Fr	Muddy Sand	Very Coarse Silty Very Fine Sand	Unimodal	Very Fine Sand	3.969	Poorly Sorted	1.938	47.0%
026_AN_S	4.25	Fr	Muddy Sand	Very Coarse Silty Very Fine Sand	Unimodal	Very Fine Sand	3.305	Poorly Sorted	1.026	22.7%
027_AN_Srg	5	Gp	Sand	Moderately Sorted Fine Sand	Unimodal	Fine Sand	2.531	Moderately Sorted	0.975	8.5%
027_AN_Srf	5	Gcm-Gmg	Muddy Sand	Very Coarse Silty Coarse Sand	Unimodal	Medium Sand	1.772	Poorly Sorted	1.618	11.7%
028_AN_S	7.25	Fr - C	Sandy Mud	Very Fine Sandy Coarse Silt	Unimodal	Coarse Silt	5.226	Poorly Sorted	1.704	82.0%
029_AN_S	9.75	Fr - C	Sandy Mud	Very Fine Sandy Very Coarse Silt	Unimodal	Very Coarse Silt	4.729	Poorly Sorted	1.565	72.9%

SAMPLE	001_AN	002_AN_S	003AM_S	04AN_D	004_AN_S	005_AN_D	006_AN_S	007_AN_S	008_AN_S	009_AN_S	010_AN_S
DATE	9/13/2021	9/13/2021	9/13/2021	9/13/2021	9/13/2021	9/13/2021	9/13/2021	9/13/2021	9/13/2021	9/13/2021	9/13/2021
SAMPLE TYPE:	Bimodal, Very Poorly Sorted	Unimodal, Poorly Sorted	Bimodal, Poorly Sorted	Unimodal, Poorly Sorted	Unimodal, Poorly Sorted	Unimodal, Poorly Sorted	Unimodal, Moderately Sorted	Unimodal, Moderately Sorted	Unimodal, Very Poorly Sorted	Unimodal, Poorly Sorted	Bimodal, Poorly Sorted
TEXTURAL GROUP:	Sandy Mud	Muddy Sand	Muddy Sand	Sandy Mud	Sandy Mud	Muddy Sand	Sand	Sand	Sandy Mud	Sandy Mud	Sandy Mud
SEDIMENT NAME:	Very Fine Sandy Coarse Silt	Very Coarse Silty Very Fine Sand	Very Coarse Silty Very Fine Sand	Very Fine Sandy Very Coarse Silt	Very Fine Sandy Very Coarse Silt	Very Coarse Silty Very Fine Sand	Moderately Sorted Fine Sand	Moderately Sorted Fine Sand	Very Fine Sandy Very Coarse Silt	Very Fine Sandy Very Coarse Silt	Very Fine Sandy Coarse Silt
FOLK AND WARD METHOD (Phi)											
MEAN (M_z):	5.088	3.945	4.021	4.291	5.017	4.023	2.698	2.333	4.645	5.224	5.284
SORTING (σ_I):	2.187	1.888	1.525	1.395	1.677	1.543	0.965	0.767	2.134	1.580	1.970
SKEWNESS (Sk_I):	0.075	0.257	0.074	0.274	0.074	0.164	0.201	0.080	0.140	0.219	(Sk_I):-0.023
KURTOSIS (K_G):	1.055	1.135	1.618	1.326	1.773	1.384	1.258	1.029	1.056	1.538	1.617
FOLK AND WARD METHOD (Description)											
MEAN:	Coarse Silt	Very Fine Sand	Very Coarse Silt	Very Coarse Silt	Coarse Silt	Very Coarse Silt	Fine Sand	Fine Sand	Very Coarse Silt	Coarse Silt	Coarse Silt
SORTING:	Very Poorly Sorted	Poorly Sorted	Poorly Sorted	Poorly Sorted	Poorly Sorted	Poorly Sorted	Moderately Sorted	Moderately Sorted	Very Poorly Sorted	Poorly Sorted	Poorly Sorted
SKEWNESS:	Symmetrical	Fine Skewed	Symmetrical	Fine Skewed	Symmetrical	Fine Skewed	Fine Skewed	Symmetrical	Fine Skewed	Fine Skewed	Symmetrical
KURTOSIS:	Mesokurtic	Leptokurtic	Very Leptokurtic	Leptokurtic	Very Leptokurtic	Leptokurtic	Leptokurtic	Mesokurtic	Mesokurtic	Very Leptokurtic	Very Leptokurtic
MODE 1 (μm):	24.61	112.5	64.72	64.72	32.44	74.31	170.2	195.4	42.76	32.44	24.61
MODE 2 (μm):	1.026		590.2								195.4
MODE 1 (ϕ):	5.348	3.156	3.953	3.953	4.950	3.754	2.558	2.359	4.551	4.950	5.348
MODE 2 (ϕ):	9.933		0.764								2.359
D_{10} (μm):	3.715	9.336	16.96	12.39	7.139	13.84	63.95	97.99	5.146	5.621	4.713
D_{50} (μm):	29.56	75.94	64.27	56.80	31.87	65.56	159.6	201.0	42.26	28.80	24.04
D_{90} (μm):	182.2	266.3	190.3	137.6	116.6	200.9	316.2	379.0	219.4	81.60	167.9
(D_{90} / D_{10}) (μm):	49.05	28.53	11.22	11.10	16.34	14.51	4.944	3.867	42.63	14.52	35.62
(D_{90} - D_{10}) (μm):	178.5	257.0	173.4	125.2	109.5	187.0	252.2	281.0	214.2	75.98	163.2
(D_{75} / D_{25}) (μm):	7.302	5.121	2.917	2.991	3.004	3.251	2.218	2.033	7.047	3.115	3.788
(D_{75} - D_{25}) (μm):	70.71	125.4	70.33	61.48	36.20	79.18	128.1	144.6	94.67	33.24	35.17
D_{10} (ϕ):	2.456	1.909	2.393	2.862	3.100	2.316	1.661	1.400	2.188	3.615	2.574
D_{50} (ϕ):	5.080	3.719	3.960	4.138	4.972	3.931	2.647	2.315	4.565	5.118	5.378
D_{90} (ϕ):	8.073	6.743	5.881	6.335	7.130	6.175	3.967	3.351	7.602	7.475	7.729
(D_{90} / D_{10}) (ϕ):	3.286	3.533	2.457	2.214	2.300	2.667	2.388	2.394	3.474	2.068	3.002
(D_{90} - D_{10}) (ϕ):	5.616	4.834	3.488	3.473	4.030	3.859	2.306	1.951	5.414	3.860	5.155
(D_{75} / D_{25}) (ϕ):	1.795	1.879	1.479	1.460	1.377	1.544	1.547	1.565	1.886	1.377	1.438
(D_{75} - D_{25}) (ϕ):	2.868	2.356	1.545	1.581	1.587	1.701	1.149	1.024	2.817	1.639	1.922
GRAIN SIZE DISTRIBUTION											
% GRAVEL:	0.0%	0.0%	0.0%	0.0%	0.0%	0.0%	0.0%	0.0%	0.0%	0.0%	0.0%
% SAND:	31.0%	56.4%	51.5%	45.0%	20.2%	52.3%	90.4%	96.2%	39.4%	16.4%	19.5%
% MUD:	69.0%	43.6%	48.5%	55.0%	79.8%	47.7%	9.6%	3.8%	60.6%	83.6%	80.5%
% V COARSE GRAVEL:	0.0%	0.0%	0.0%	0.0%	0.0%	0.0%	0.0%	0.0%	0.0%	0.0%	0.0%
% COARSE GRAVEL:	0.0%	0.0%	0.0%	0.0%	0.0%	0.0%	0.0%	0.0%	0.0%	0.0%	0.0%
% MEDIUM GRAVEL:	0.0%	0.0%	0.0%	0.0%	0.0%	0.0%	0.0%	0.0%	0.0%	0.0%	0.0%
% FINE GRAVEL:	0.0%	0.0%	0.0%	0.0%	0.0%	0.0%	0.0%	0.0%	0.0%	0.0%	0.0%
% V FINE GRAVEL:	0.0%	0.0%	0.0%	0.0%	0.0%	0.0%	0.0%	0.0%	0.0%	0.0%	0.0%
% V COARSE SAND:	0.0%	0.0%	0.0%	0.0%	0.0%	0.0%	0.0%	0.0%	0.0%	0.0%	0.0%
% COARSE SAND:	0.4%	1.2%	4.2%	0.7%	1.3%	1.6%	0.2%	2.0%	0.7%	0.1%	1.5%
% MEDIUM SAND:	5.2%	10.2%	3.8%	1.3%	4.3%	5.4%	20.9%	31.8%	7.1%	1.4%	4.9%
% FINE SAND:	10.9%	21.1%	11.3%	11.0%	4.0%	14.8%	44.6%	47.1%	14.3%	3.4%	6.0%
% V FINE SAND:	14.4%	23.8%	32.2%	32.1%	10.6%	30.5%	24.7%	15.2%	17.3%	11.4%	7.1%
% V COARSE SILT:	17.5%	18.1%	28.4%	29.6%	30.8%	25.9%	4.7%	1.7%	18.8%	29.6%	19.4%
% COARSE SILT:	18.8%	10.7%	10.8%	13.1%	28.3%	10.8%	2.2%	1.7%	16.8%	29.2%	28.9%
% MEDIUM SILT:	14.4%	6.1%	3.8%	5.5%	10.1%	4.7%	0.9%	0.4%	11.1%	12.4%	17.4%
% FINE SILT:	7.9%	3.6%	1.9%	2.6%	3.6%	2.5%	0.5%	0.0%	5.7%	4.3%	5.8%
% V FINE SILT:	4.4%	2.3%	1.2%	1.5%	2.5%	1.5%	0.5%	0.0%	3.2%	2.7%	3.1%
% CLAY:	6.0%	2.9%	2.5%	2.7%	4.4%	2.3%	0.9%	0.0%	5.0%	5.4%	5.9%

SAMPLE	011_AN_S	012_AN_S	013_AN_S	014_AN_S	015_AN_S	016_AN_S	017_AN_S	018_AN_S	019_AN_S	020_AN_S
DATE	9/13/2021	9/13/2021	9/13/2021	9/13/2021	9/13/2021	9/13/2021	9/13/2021	9/13/2021	9/13/2021	9/13/2021
SAMPLE TYPE:	Bimodal, Very Poorly Sorted	Bimodal, Poorly Sorted	Bimodal, Very Poorly Sorted	Unimodal, Poorly Sorted	Unimodal, Very Poorly Sorted	Bimodal, Very Poorly Sorted	Bimodal, Very Poorly Sorted	Unimodal, Poorly Sorted	Bimodal, Very Poorly Sorted	Unimodal, Moderately Sorted
TEXTURAL GROUP:	Sandy Mud	Sandy Mud	Sandy Mud	Muddy Sand	Sandy Mud	Sandy Mud	Sandy Mud	Sandy Mud	Sandy Mud	Sand
SEDIMENT NAME:	Fine Sandy Coarse Silt	Fine Sandy Coarse Silt	Very Fine Sandy Coarse Silt	Very Coarse Silty Medium Sand	Very Fine Sandy Coarse Silt	Fine Sandy Coarse Silt	Very Fine Sandy Coarse Silt	Very Fine Sandy Very Coarse Silt	Fine Sandy Coarse Silt	Moderately Sorted Fine Sand
FOLK AND WARD METHOD (Phi)										
MEAN (M_z):	5.086	5.603	4.962	2.303	4.928	5.113	4.866	5.209	5.070	2.570
SORTING (σ_I):	2.196	1.927	2.152	1.765	2.079	2.596	2.011	1.438	2.205	0.792
SKEWNESS	-0.097	0.007	-0.048	0.430	0.067	-0.111	-0.004	0.231	-0.007	(Sk_I): 0.081
KURTOSIS (K_G):	1.390	1.660	1.535	1.441	1.225	0.888	1.308	1.591	1.112	0.994
FOLK AND WARD METHOD (Description)										
MEAN:	Coarse Silt	Coarse Silt	Very Coarse Silt	Fine Sand	Very Coarse Silt	Coarse Silt	Very Coarse Silt	Coarse Silt	Coarse Silt	Fine Sand
SORTING:	Very Poorly Sorted	Poorly Sorted	Very Poorly Sorted	Poorly Sorted	Very Poorly Sorted	Very Poorly Sorted	Very Poorly Sorted	Poorly Sorted	Very Poorly Sorted	Moderately Sorted
SKEWNESS:	Symmetrical	Symmetrical	Symmetrical	Very Fine Skewed	Symmetrical	Coarse Skewed	Symmetrical	Fine Skewed	Symmetrical	Symmetrical
KURTOSIS:	Leptokurtic	Very Leptokurtic	Very Leptokurtic	Leptokurtic	Leptokurtic	Platykurtic	Leptokurtic	Very Leptokurtic	Leptokurtic	Mesokurtic
MODE 1 (µm):	21.43	21.43	28.25	390.0	28.25	16.26	28.25	32.44	24.61	170.2
MODE 2 (µm):	195.4	224.4	195.4			224.4	170.2		170.2	
MODE 1 (ϕ):	5.548	5.548	5.149	1.362	5.149	5.946	5.149	4.950	5.348	2.558
MODE 2 (ϕ):	2.359	2.159	2.359			2.159	2.558		2.558	
D_{10} (µm):	4.478	3.812	4.808	26.17	4.550	2.841	5.602	6.668	3.753	80.82
D_{50} (µm):	24.26	20.42	28.38	249.0	32.44	22.37	31.09	29.01	26.69	171.4
D_{90} (µm):	222.1	138.1	234.2	595.5	187.4	297.2	195.9	72.27	199.4	329.9
(D_{90} / D_{10}) (µm):	49.60	36.23	48.72	22.75	41.18	104.6	34.97	10.84	53.12	4.081
(D_{90} - D_{10}) (µm):	217.6	134.3	229.4	569.3	182.8	294.4	190.3	65.60	195.6	249.0
(D_{75} / D_{25}) (µm):	4.899	3.655	4.379	3.751	5.473	13.98	4.756	2.759	6.630	2.109
(D_{75} - D_{25}) (µm):	46.71	28.25	48.13	313.1	63.96	111.7	57.35	29.58	66.11	129.4
D_{10} (ϕ):	2.171	2.856	2.094	0.748	2.416	1.750	2.352	3.791	2.327	1.600
D_{50} (ϕ):	5.365	5.614	5.139	2.006	4.946	5.482	5.007	5.107	5.228	2.545
D_{90} (ϕ):	7.803	8.035	7.700	5.256	7.780	8.459	7.480	7.228	8.058	3.629
(D_{90} / D_{10}) (ϕ):	3.594	2.813	3.677	7.028	3.220	4.833	3.180	1.907	3.463	2.268
(D_{90} - D_{10}) (ϕ):	5.632	5.179	5.606	4.508	5.364	6.709	5.128	3.438	5.731	2.029
(D_{75} / D_{25}) (ϕ):	1.560	1.399	1.532	2.553	1.667	2.246	1.595	1.331	1.741	1.532
(D_{75} - D_{25}) (ϕ):	2.293	1.870	2.131	1.907	2.452	3.806	2.250	1.464	2.729	1.077
GRAIN SIZE DISTRIBUTION										
% GRAVEL:	0.0%	0.0%	0.0%	0.0%	0.0%	0.0%	0.0%	0.0%	0.0%	0.0%
% SAND:	24.1%	15.7%	25.0%	84.4%	30.2%	32.3%	28.1%	13.7%	28.4%	95.0%
% MUD:	75.9%	84.3%	75.0%	15.6%	69.8%	67.7%	71.9%	86.3%	71.6%	5.0%
% V COARSE GRAVEL:	0.0%	0.0%	0.0%	0.0%	0.0%	0.0%	0.0%	0.0%	0.0%	0.0%
% COARSE GRAVEL:	0.0%	0.0%	0.0%	0.0%	0.0%	0.0%	0.0%	0.0%	0.0%	0.0%
% MEDIUM GRAVEL:	0.0%	0.0%	0.0%	0.0%	0.0%	0.0%	0.0%	0.0%	0.0%	0.0%
% FINE GRAVEL:	0.0%	0.0%	0.0%	0.0%	0.0%	0.0%	0.0%	0.0%	0.0%	0.0%
% V FINE GRAVEL:	0.0%	0.0%	0.0%	0.0%	0.0%	0.0%	0.0%	0.0%	0.0%	0.0%
% V COARSE SAND:	0.0%	0.0%	0.0%	0.0%	0.0%	0.0%	0.0%	0.0%	0.0%	0.0%
% COARSE SAND:	1.9%	1.1%	2.9%	17.5%	1.0%	2.6%	0.8%	0.1%	0.1%	0.3%
% MEDIUM SAND:	6.6%	4.3%	6.5%	32.3%	5.4%	10.4%	5.9%	1.8%	6.2%	23.8%
% FINE SAND:	8.1%	5.2%	6.7%	23.0%	9.9%	11.4%	9.8%	2.5%	11.7%	47.0%
% V FINE SAND:	7.4%	5.1%	8.9%	11.5%	14.0%	7.8%	11.6%	9.3%	10.4%	23.9%
% V COARSE SILT:	16.7%	16.5%	21.2%	4.8%	21.0%	10.1%	21.7%	32.2%	16.5%	3.5%
% COARSE SILT:	25.9%	29.3%	26.2%	2.7%	21.6%	17.3%	24.5%	31.4%	22.5%	1.0%
% MEDIUM SILT:	17.6%	20.7%	13.8%	2.5%	12.3%	17.3%	12.9%	11.5%	15.1%	0.4%
% FINE SILT:	6.7%	7.6%	5.0%	2.4%	5.8%	10.1%	4.9%	3.9%	7.2%	0.0%
% V FINE SILT:	3.3%	3.6%	3.0%	1.7%	3.6%	5.7%	3.0%	2.5%	4.4%	0.0%
% CLAY:	5.8%	6.6%	5.8%	1.5%	5.4%	7.2%	4.9%	4.8%	5.9%	0.0%

SAMPLE	021_AN_S	022_AN_S	023_AN_S	024_AN_S	025_AN_S	026_AN_S	027_AN_SFg	027_AN_SFf	028_AN_S	029_AN_S
DATE	9/13/2021	9/13/2021	9/13/2021	9/13/2021	9/13/2021	9/13/2021	9/13/2021	9/13/2021	9/13/2021	9/13/2021
SAMPLE TYPE:	Unimodal, Poorly Sorted	Unimodal, Poorly Sorted	Unimodal, Poorly Sorted	Unimodal, Moderately Sorted	Unimodal, Poorly Sorted	Unimodal, Poorly Sorted	Unimodal, Moderately Sorted	Unimodal, Poorly Sorted	Unimodal, Poorly Sorted	Unimodal, Poorly Sorted
TEXTURAL GROUP:	Muddy Sand	Muddy Sand	Muddy Sand	Sand	Muddy Sand	Muddy Sand	Sand	Muddy Sand	Sandy Mud	Sandy Mud
SEDIMENT NAME:	Very Coarse Silty Medium Sand	Very Coarse Silty Very Fine Sand	Very Coarse Silty Medium Sand	Moderately Sorted Fine Sand	Very Coarse Silty Very Fine Sand	Very Coarse Silty Very Fine Sand	Moderately Sorted Fine Sand	Very Coarse Silty Coarse Sand	Very Fine Sandy Coarse Silt	Very Fine Sandy Very Coarse Silt
FOLK AND WARD METHOD (Phi)										
MEAN (M_z):	1.795	3.633	2.335	2.650	3.969	3.305	2.531	1.772	5.226	4.729
SORTING (σ_I):	1.620	1.201	1.380	0.950	1.938	1.026	0.975	1.618	1.704	1.565
SKEWNESS	0.496	0.182	0.307	0.144	0.162	0.164	0.159	0.423	0.126	0.149
KURTOSIS (K_G):	1.533	1.153	1.234	1.126	1.075	1.168	1.131	1.229	1.591	1.684
FOLK AND WARD METHOD (Description)										
MEAN:	Medium Sand	Very Fine Sand	Fine Sand	Fine Sand	Very Fine Sand	Very Fine Sand	Fine Sand	Medium Sand	Coarse Silt	Very Coarse Silt
SORTING:	Poorly Sorted	Poorly Sorted	Poorly Sorted	Moderately Sorted	Poorly Sorted	Poorly Sorted	Moderately Sorted	Poorly Sorted	Poorly Sorted	Poorly Sorted
SKEWNESS:	Very Fine Skewed	Fine Skewed	Very Fine Skewed	Fine Skewed	Fine Skewed	Fine Skewed	Fine Skewed	Very Fine Skewed	Fine Skewed	Fine Skewed
KURTOSIS:	Very Leptokurtic	Leptokurtic	Leptokurtic	Leptokurtic	Mesokurtic	Leptokurtic	Leptokurtic	Leptokurtic	Very Leptokurtic	Very Leptokurtic
MODE 1 (μm):	514.1	97.96	295.8	170.2	74.31	112.5	195.4	514.1	28.25	42.76
MODE 2 (μm):										
MODE 1 (ϕ):	0.963	3.355	1.761	2.558	3.754	3.156	2.359	0.963	5.149	4.551
MODE 2 (ϕ):										
D_{10} (μm):	43.95	25.77	46.13	65.72	9.743	38.17	69.37	51.43	5.569	8.808
D_{50} (μm):	368.4	85.08	224.6	164.1	68.86	105.7	179.1	372.3	28.01	39.60
D_{90} (μm):	748.6	203.9	526.4	340.6	296.7	226.3	373.3	852.7	97.79	116.9
(D_{90} / D_{10}) (μm):	17.03	7.912	11.41	5.183	30.45	5.928	5.381	16.58	17.56	13.27
(D_{90} - D_{10}) (μm):	704.7	178.1	480.2	274.9	286.9	188.1	303.9	801.3	92.23	108.1
(D_{75} / D_{25}) (μm):	3.120	2.825	3.094	2.300	5.730	2.409	2.351	3.752	3.316	2.890
(D_{75} - D_{25}) (μm):	385.1	89.30	249.1	138.4	131.0	93.25	154.5	448.4	34.78	42.98
D_{10} (ϕ):	0.418	2.294	0.926	1.554	1.753	2.144	1.422	0.230	3.354	3.097
D_{50} (ϕ):	1.441	3.555	2.154	2.607	3.860	3.242	2.481	1.426	5.158	4.658
D_{90} (ϕ):	4.508	5.278	4.438	3.927	6.681	4.711	3.850	4.281	7.488	6.827
(D_{90} / D_{10}) (ϕ):	10.79	2.301	4.794	2.528	3.811	2.198	2.708	18.63	2.233	2.205
(D_{90} - D_{10}) (ϕ):	4.090	2.984	3.512	2.374	4.928	2.568	2.428	4.051	4.134	3.730
(D_{75} / D_{25}) (ϕ):	3.004	1.525	2.130	1.592	1.948	1.479	1.651	3.687	1.400	1.390
(D_{75} - D_{25}) (ϕ):	1.642	1.498	1.630	1.202	2.518	1.269	1.233	1.908	1.729	1.531
GRAIN SIZE DISTRIBUTION										
% GRAVEL:	0.0%	0.0%	0.0%	0.0%	0.0%	0.0%	0.0%	0.0%	0.0%	0.0%
% SAND:	87.7%	65.2%	86.8%	90.9%	53.0%	77.3%	91.5%	88.3%	18.0%	27.1%
% MUD:	12.3%	34.8%	13.2%	9.1%	47.0%	22.7%	8.5%	11.7%	82.0%	72.9%
% V COARSE GRAVEL:	0.0%	0.0%	0.0%	0.0%	0.0%	0.0%	0.0%	0.0%	0.0%	0.0%
% COARSE GRAVEL:	0.0%	0.0%	0.0%	0.0%	0.0%	0.0%	0.0%	0.0%	0.0%	0.0%
% MEDIUM GRAVEL:	0.0%	0.0%	0.0%	0.0%	0.0%	0.0%	0.0%	0.0%	0.0%	0.0%
% FINE GRAVEL:	0.0%	0.0%	0.0%	0.0%	0.0%	0.0%	0.0%	0.0%	0.0%	0.0%
% V FINE GRAVEL:	0.0%	0.0%	0.0%	0.0%	0.0%	0.0%	0.0%	0.0%	0.0%	0.0%
% V COARSE SAND:	1.1%	0.0%	0.0%	0.0%	0.0%	0.0%	0.0%	5.1%	0.0%	0.0%
% COARSE SAND:	31.5%	0.0%	11.8%	1.1%	2.1%	0.7%	2.3%	30.4%	0.0%	0.8%
% MEDIUM SAND:	33.8%	5.0%	32.8%	22.8%	11.5%	6.6%	26.8%	29.4%	3.1%	3.5%
% FINE SAND:	14.9%	24.9%	28.9%	42.8%	18.2%	32.2%	41.6%	14.7%	4.7%	4.9%
% V FINE SAND:	6.5%	35.2%	13.3%	24.2%	21.2%	37.8%	20.7%	8.7%	10.1%	17.9%
% V COARSE SILT:	4.1%	21.8%	6.1%	5.4%	19.3%	15.2%	4.8%	4.8%	26.9%	34.9%
% COARSE SILT:	2.6%	7.3%	3.1%	2.0%	12.7%	4.2%	2.0%	2.5%	28.9%	22.1%
% MEDIUM SILT:	1.5%	2.4%	1.6%	0.9%	6.7%	1.7%	0.9%	1.7%	13.5%	6.5%
% FINE SILT:	1.1%	1.1%	1.0%	0.6%	3.5%	0.8%	0.5%	1.1%	4.7%	3.2%
% V FINE SILT:	1.2%	0.6%	0.6%	0.3%	2.1%	0.4%	0.2%	0.7%	2.8%	2.1%
% CLAY:	1.9%	1.6%	0.8%	0.0%	2.7%	0.3%	0.0%	1.0%	5.2%	4.0%